

STUDY REPORT

SR 228 (2010)

STUDY OF THE MOISTURE MANAGEMENT PROPERTIES OF ROOF UNDERLAYS

Luca Quaglia

Malcolm Cunningham



The work reported here was jointly funded by BRANZ from the Building Research Levy, and the Department of Building and Housing.

Preface

This is the third and final report prepared during research into the role of roof underlays for moisture management in roof spaces. The report describes the physical properties of a range of roof underlays, the results of field and laboratory experiments aimed at studying the role of underlays in managing moisture, and an analytical model reproducing some of the experimental results. The proposal for a new test, called “Surface Water No Drip Test”, is also described. This could replace the current “absorbency test”.

Acknowledgments

This work was jointly funded by the Building Research Levy and the Department of Building and Housing.

Note

This report is intended for other researchers interested in moisture management in roof spaces.

Study of the Moisture Management Properties of Roof Underlays

BRANZ Study Report SR 228

L. Quaglia

M. J. Cunningham

Reference

Quaglia L. and Cunningham M. 2010. 'Study of the Moisture Management Properties of Roof Underlays'. BRANZ *Study Report* 228. BRANZ Ltd, Judgeford, New Zealand.

EXECUTIVE SUMMARY

Roof underlays are an integral part of moisture management strategies for roof spaces. Roof claddings constitute the first line of defence against the elements and roof underlays the second one. Moreover roof underlays play an important role in managing moisture which can accumulate in the interstices of the roof envelope.

Several mechanisms can give rise to interstitial moisture in the roof envelope. Some pertain to the normal behaviour of roof assemblies and some originate from minor or major failures or design faults. The main function of roof underlays is to prevent timber framing and insulation from getting wet. Timber framing exposed to excessive moisture can decay quite rapidly and reduce the lifespan of the roof assembly. Wet insulation has a reduced R-value and severely compromises the thermal properties of the roof assembly.

In this study we explore some of the moisture management properties of roof underlays to ascertain what their role is and to identify what physical properties underlays are required to have in order to accomplish that role. The final aim of this research effort is to design pliable building membrane tests that reflect the “real world” behaviour of roof underlays.

In order to study roof underlays experiments have been made, both in an especially built test house and in the laboratory, and a hygrothermal model has been developed to interpret some of the measurements.

In the case of metal roofs, the received wisdom is that when condensation accumulates on the underside of the cladding (for example during calm frosty nights), it will drip onto the underlay and eventually run down it. This line of thought continues with the requirement that the underlay has to be absorbent in order to retain the dripping condensate until the weather conditions improve.

It was found that when condensation does form on the underside of the metal cladding, it begins as small water droplets which then coalesce into big droplets. These droplets do not drip but stay localised by the action of surface tension or slide towards the lowest regions of the metal profile. Condensation forming on the underside of the metal thus ends up sitting in contact with the upper surface of the underlay under the lowest regions of the metal profile, without evident signs of dripping and limited evidence of draining down the underlay.

The underlay has to be able to prevent the water from being transferred to the layers underneath. Two properties of the underlay deal with retaining water which forms or accumulates on the upper side of the underlay: liquid penetration resistance and absorbency. Liquid penetration resistance characterises the ability of the underlay to withstand a 100 mm column of water without having water seeping through to the other side. Absorbency is the ability to retain water in the body of the underlay.

Field and laboratory experiments were conducted to study the relative importance of these two properties in managing moisture accumulating or forming on the upper side of the underlay. Liquid penetration resistance is the main property that a roof underlay is required to have, with absorbency playing only a minor role. Water accumulating or forming on the upper surface of the underlay stays localised or eventually runs down the underlay, but is not transferred to the lower layers of the roof envelope.

Condensation can also accumulate on the underside of the underlay. Modelling has shown that the presence of the underlay reduces the amount of condensation appearing on the underside of the cladding and that much of the condensation does indeed form on the underside of the underlay. The underlay has to be able to hold this condensation, mainly by surface tension, so that it does not drip deeper in the roof structure.

From the experimental and theoretical results, the two most important moisture-related properties required by a roof underlay are liquid penetration resistance and the ability to hold condensation on the underside.

The AS/NZS 4201 test “Resistance to water penetration” is well adequate to measure the first property. The requirement to be able to withhold 100 mm of water far exceeds any likely head of water that condensation on the upper side of the underlay could be able to exert (just a few millimetres). A limit of 100 mm is recommendable in order to offer some protection to the roof framing in case of water leaks following a major failure of the roof cladding.

The second property calls for a new test that we have called “surface water no-drip test”. The test consists of generating condensation on the underside of an underlay specimen until drip starts. The amount of condensation before drip starts is the quantity measured by the test. This quantity has to be greater than the likely quantity of condensation that could form under very severe New Zealand weather conditions. Modelling sets a safe limit to 100 g/m².

The traditional requirement for roof underlays to have an absorbency (defined according to the Standard AS/NZS 4201) of at least 100 g/m² has not been found very relevant in any of the different experiments, test and modelling performed. On the contrary, the requirement to be water vapour permeable is relevant for the overall hygrothermal behaviour of the roof envelope.

In conclusion, all test in Standards AS/NZS 4201 and NZS 2295, except for the absorbency test, have been found to serve a useful purpose. It is proposed to adopt a new test, the “surface water no-drip test”, to probe an important task a roof underlay should be able to perform.

Solar-driven moisture has also been investigated. If the roof cladding is absorbent (like in the case of porous concrete tiles), it can store a considerable amount of water after rain events. When solar radiation shines on the wet cladding, it evaporates most of the water stored in it but also drives a fraction of the water towards the inside of the roof envelope. This moisture is called “solar-driven moisture”. Roof underlays are not required to be installed under an absorbent cladding but there is an argument saying that they could be useful in order to deal with solar-driven moisture. Experiments have shown that solar-driven moisture is negligible, supporting the claim that roof underlays are not required under absorbent roof claddings.

Contents	Page
1. INTRODUCTION	1
1.1 Mechanisms pertaining to the normal behaviour of a roof.....	4
1.2 Mechanisms pertaining to the pathological behaviour of a roof	5
2. PROPERTIES OF A RANGE OF ROOF UNDERLAYS	6
2.1 Introduction	6
2.2 Area density	6
2.3 Water vapour resistance	7
2.4 Water absorbency	8
2.5 Liquid penetration resistance.....	8
2.6 Air resistance	8
3. SOME OBSERVED PHENOMENA DURING FIELD EXPERIMENTS	10
3.1 Introduction	10
3.2 Evidence of night sky radiative cooling	10
3.3 Negative observation of solar-driven moisture	15
3.4 CONCLUSION.....	17
4. DRY ICE RESULTS	18
4.1 Introduction	18
4.2 Results and observations of the dry ice experiments.....	20
4.3 Conclusions	24
5. AN EXPERIMENT TO EXAMINE STUDY UPPER SURFACE LIQUID.....	25
5.1 Introduction	25
5.2 Set-up of upper surface liquid experiment.....	25
5.3 Results of the upper surface liquid experiment	27
5.4 Conclusions	28
6. AN ANALYTICAL MODEL TO EXAMINE THE EFFECT OF UNDERLAYS ON CONDENSATION RATES UNDER METAL ROOFS.....	29
6.1 Model description.....	29
6.1.1 High and low hygroscopic papers.....	29
6.1.2 Model equations	31
6.2 Condensation mechanisms – no underlay	33
6.3 Condensation mechanisms – high hygroscopy.....	34
6.3.1 Suppression of roof condensation by hygroscopic damping of the local relative humidity	34
6.3.2 Reduction of condensation rate through hygroscopic absorption	35
6.3.3 Prevention of contact of lower cavity air with the roof	36
6.4 Condensation mechanisms – low hygroscopy	37
6.5 Examples.....	37
6.5.1 Skillion roof with a Kraft underlay.....	37
6.5.2 Non-hygroscopic underlay.....	38
7. STUDY OF ROOF UNDERLAY ACTING AS A CONDENSATION PLANE	43

7.1	Introduction	43
7.2	Climate chamber condensation experiment	43
7.3	Experimental results: condensation on the underside of the metal plate	46
7.4	Experimental results: condensation on the underside of the underlay	47
7.5	Measurement of mass transfer coefficients	51
7.6	Conclusions	52
8.	PROPOSAL FOR A NEW “SURFACE WATER NO-DRIP TEST”	53
8.1	Introduction	53
8.2	Description of the experimental set-up	53
8.3	Some theoretical considerations	53
8.4	Results of the Surface water no-drip test	55
8.5	Threshold for the Surface water no-drip test	56
8.6	Conclusions	58
9.	SUMMARY OF FINDINGS	59
9.1	Condensation	59
9.2	Solar driven moisture transfer	59
	APPENDIX A SURFACE WATER NO-DRIP TEST	60

Figures	Page
Figure 1: Example of night sky radiative cooling during cloudless and still nights when the temperature of the cladding can significantly drop below ambient temperature	11
Figure 2: Picture of the condensation apparatus for roofs clad with metal sheets	12
Figure 3: Picture of the condensation apparatus for roofs clad with tiles	12
Figure 4: Another example of night sky radiative cooling (the corresponding gravimetric measurements are presented in Figure 5)	13
Figure 5: Gravimetric condensation measurements during the night sky radiative cooling presented in Figure 4. The weight of the section of underlay (part of the condensation apparatus) was measured at regular intervals during the event, then it was converted to moisture content using the area density of the dry material reported in Table 1.....	14
Figure 6: Difference between the weight of the modified tile of the condensation apparatus after watering the roof specimen and its weight just before starting watering the roof (called “initial weight”). One roof specimen was watered during more than 18 hours (simulating the equivalent of 100 mm of rain) and one was left dry. The graph represents the evolution of the weights after the watering was stopped and while solar radiation dried the roof	15
Figure 7: Difference between the weight of the section of underlay of the condensation apparatus after watering the roof specimen and its weight just before starting watering the roof (called “initial weight”). One roof specimen was watered during more than 18 hours (simulating the equivalent of 100 mm of rain) and one was left dry	16
Figure 8: Evolution of the relative humidity in the cavity between underlay and cladding during the final phase of the watering and during the drying of the roof specimens. One roof specimen was watered for 18 hours simulating the equivalent of 100 mm of rain and one was left dry. The sun rose at around 6.30am and the watering was stopped at around 11am	17
Figure 9: Metallic frame used to support the dry ice pellets in the dry ice experiment.....	19

Figure 10: Polystyrene enclosure surrounding the metallic frame during the dry ice experiment. During the experiment thick polystyrene sheets sit on the polystyrene enclosure and cover the metallic frame in order to create an insulated cavity above the metal cladding.	19
Figure 11: Initial condition of the cavity between corrugated metal cladding and underlay. The picture was taken using a boroscope and the point of view is looking across the short length of the cavity	20
Figure 12:Condition of the cavity 10-15 minutes after the start of the dry ice experiment. The underside of the metal cladding is covered by a thin layer of frost.....	21
Figure 13: Condition of the cavity 30-40 minutes after the start of the dry ice experiment. The underside of the metal cladding is covered by a thick layer of frost	21
Figure 14: After removing the dry ice, the layer of frost starts to melt nearly immediately	22
Figure 15: After the layer of ice has quickly melted, the surface of the metal is covered by fine water drops	22
Figure 16:The fine water droplets soon coalescent into big drops, especially near the lower parts of the metal profile	23
Figure 17: Condensation accumulates near the valleys of the corrugated metal profile	23
Figure 18: Set-up for the upper surface liquid experiment. An underlay specimen is mounted on a sloping metallic frame which is placed in a climate chamber. A set of small plastic tubes connected to a peristaltic pump provide a source of condensation forming in contact to the upper surface of the underlay.....	26
Figure 19: Detail of the manifold which artificially creates contact liquid on the top edge of the underlay specimen	27
Figure 20:Roof types and model nodes	30
Figure 21: Model diagram	31
Figure 22:Model of a roof system without an underlay.....	33
Figure 23 An example of the reduction of roof condensation rate for low hygroscopy underlays as a function of underlay vapour resistance	37
Figure 24: Vapour pressures with Kraft paper. The vertical dashed lines mark the boundaries between the three regimes (see text).....	40
Figure 25: Condensation and condensation rates with kraft paper. The vertical dashed lines mark the boundaries between the three regimes, see text.	40
Figure 26: Condensation with Kraft paper on the underlay, the roof, and in the case of no underlay. The vertical dashed lines mark the boundaries between the three regimes (see text)	41
Figure 27: Vapour pressures with non-hygroscopic underlay	41
Figure 28: Condensation and condensation rates with non-hygroscopic underlay	42
Figure 29: Condensation with low hygroscopy underlay, on the underlay, the roof, and in the case of no underlay	42
Figure 30: Metal frame used to support the underlay specimen. The sides of the metal frame are sealed to create a confined space. A tray of water with a flat heater provides the source of moisture.....	44
Figure 31:The underlay specimen clamped to the metal frame. This set-up aims to reproduce the equivalent of a very moist roof space.....	45
Figure 32: Polystyrene enclosure supporting a metal plate and creating a cavity above the underlay specimen	45
Figure 33: Metal plate simulating a metal cladding installed above the underlay specimen ..	46
Figure 34: Condensation accumulation on the underside of the metal plate during the climate chamber condensation experiment.	48

Figure 35: Condensation accumulation on the underside of the underlay for several membranes during the climate chamber condensation experiment.....	48
Figure 36: Comparison between the hygroscopic sorption curve of a synthetic wrap (Wrap C) and a paper-based wrap (Wrap F)	49
Figure 37: Schematic of the driving forces creating an accumulation of condensation on the underside of the underlay. The vapour pressures depend on the temperature T and on the RH. The surface mass transfer coefficient is represented by the constant h. The condensation rate is then proportional to the surface mass transfer coefficient and to the differential in vapour pressures	50
Figure 38: Thermal conditions near the underside of underlay specimens during the climate chamber condensation experiment	50
Figure 39: Hygroscopic conditions near the underside of the underlay specimen in the climate chamber condensation experiment.....	51
Figure 40: Experimental set-up for "Surface water no-drip test"	54
Figure 41: Detail of the Plexiglas frame supporting the underlay. The specimen is attached simply using double tape.....	54
Figure 42: Part of the equipment controlling and logging the "Surface water no-drip test"	55
Figure 43: Theoretical interpretation of the surface water no drip test	56
Figure 44 Surface water no-drip test: mass increase of different underlay samples.....	57
Figure 45 Surface water no-drip test: mass loss due to drip	58
Figure 46: Thin square Plexiglas holding frame (no specimen attached)	65
Figure 47:Thin square Plexiglas holding frame with specimen to test attached.....	65
Figure 48: Experimental set-up. From top to bottom: scale sitting on scale frame, Plexiglas holding frame with specimen to test, container with distilled water and resistive heater.....	66
Figure 49: Detail of the underside hook of the scale supporting the Plexiglas holding frame with specimen to test.....	66

Tables	Page
Table 1 Dry area density of a range of building wraps	7
Table 2 Water vapour resistance of a range of building wraps	7
Table 4 Liquid penetration resistance of a range of building wraps	9
Table 5 Air resistance of a range of building wraps. Air resistance is measured with a Gurley apparatus. The description "impermeable" indicates that the air resistance is higher than the maximum value measurable with a Gurley machine. The description "too porous" indicates that the air resistance was lower than the minimum value measurable with a Gurley machine. The description "leaked" indicates that the surface of the wrap does not allow clamping of the Gurley machine in order to conduct an accurate measurement.....	9
Table 6 Underlay (non-hygroscopic) parameters	38
Table 7 Thermal properties of the example roof	38
Table 8 Example roof parameters	39
Table 9: Psychrometric parameters	39
Table 10: Underlay (hygroscopic) parameters	39
Table 11 Surface mass transfer coefficient of a range of building wraps.....	52

Table 12 Results of the surface water no-drip test for several roof underlays. The condensation accumulation is the maximum amount of condensation that can be held by surface tension by a roof underlay in a horizontal position before drip starts 57

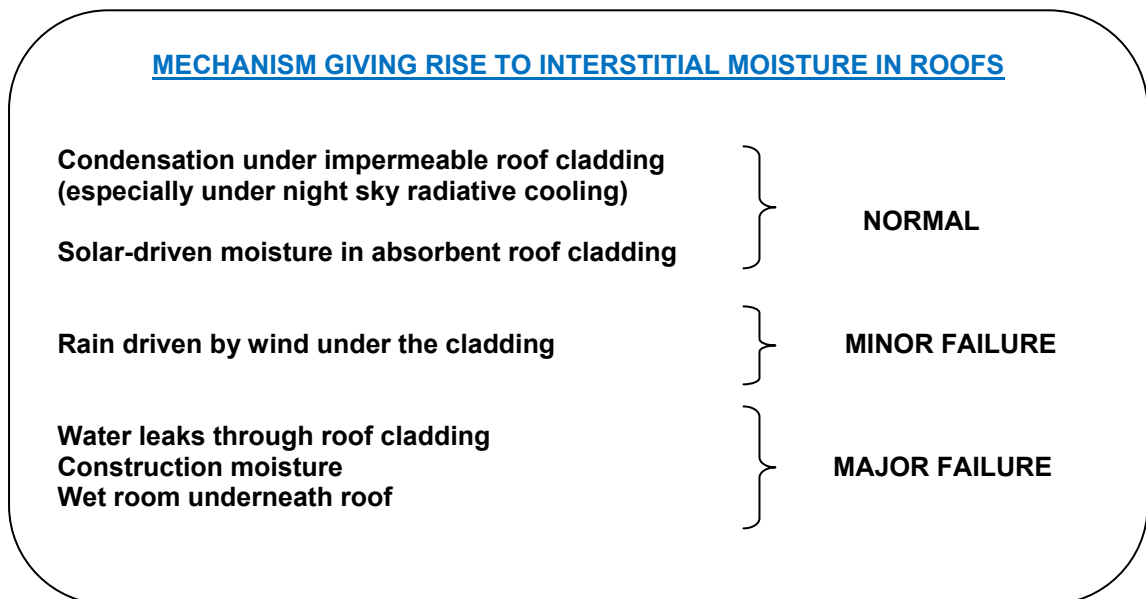
1. INTRODUCTION

Roof underlays are an integral part of moisture management strategies for roof spaces. Roof claddings constitute the first line of defence against the elements and roof underlays the second one. Moreover roof underlays play an important role in managing moisture which can form in the interstices of the roof.

Several mechanisms can give rise to interstitial moisture. Some pertain to the normal behaviour of roof assemblies and some originate from minor or major failures or design faults. The main function of roof underlays is to prevent, in ways that will be examined in detail in this report, timber framing and insulation from getting wet. Timber framing exposed to excessive moisture can decay quite rapidly and reduce the lifespan of the roof assembly. Wet insulation has a reduced R-value and severely compromises the thermal properties of the roof assembly.

In this study we aim to explore some of the moisture management properties of roof underlays to ascertain what their role is and to identify what physical properties underlays are required to have in order to accomplish that role.

As a guideline for the reader, we give a flow chart of the different ideas and reasons which have shaped this study.



WHAT FUNCTION DO ROOF UNDERLAYS PLAY IN MANAGING INTERSTITIAL MOISTURE?

MAIN FUNCTION OF UNDERLAY

Prevent roof members and insulation from getting wet
by retaining or diverting water or
by reducing moisture accumulation

HOW DO UNDERLAYS BEHAVE IN THE FIELD?

FIELD EXPERIMENTS

Night Sky Radiation → Condensation on impermeable cladding
Solar-driven moisture → Condensation from absorbent cladding

VERY LITTLE CONDENSATION OBSERVED

NEED TO ACHIEVE MORE EXTREME CONDITIONS TO OBSERVE DYNAMICS OF CONDENSATION

DRY ICE EXPERIMENT

DYNAMICS OF CONDENSATION ON IMPERMEABLE CLADDING: condensation on metal cladding starts as thin film, then small droplets which coalesce into big droplets, which then slide towards lower points of metal profile

NO EVIDENT SIGN OF DRIP

NEED TO PERFORM LABORATORY EXPERIMENT TO STUDY DRIPPING

ARTIFICIAL CONTACT BETWEEN WATER AND TOP SURFACE OF UNDERLAY

Water droplets sit on top of the underlay or run down the underlay

Running water droplets are rarely absorbed (even in the case of underlays considered highly absorbent according to the test prescribed by Standard NZS 2295)

Even after extended periods of contact, no water droplets were able to percolate through the body of the underlay

**TO DEAL WITH MOISTURE SITTING OR RUNNING ON THE TOP SURFACE OF THE UNDERLAY
THE MOST IMPORTANT PROPERTY OF UNDERLAY IS LIQUID PENETRATION RESISTANCE**

The liquid penetration resistance test prescribed by Standard NZS 2295 is suitable to probe the ability of an underlay to cope with dripping

**CONDENSATION COULD FORM ON THE UNDERSIDE (SEEN IN MODEL) OF THE UNDERLAY AND DRIP
NEED TO INVESTIGATE THE CASE OF UNDERLAY ACTING AS A CONDENSATION PLANE**

CONDENSATION EXPERIMENTS IN CLIMATE CHAMBER

DYNAMICS OF CONDENSATION ON UNDERSIDE OF UNDERLAY: during the hygroscopic phase, moisture is stored in the body of the underlay. Paper-based products have larger storing hygroscopic capability than synthetic products which have a very limited one. Beyond that phase, condensation initially appears as a thin film, then a layer of fine droplets, and finally as a layer of large droplets which are held in place just by surface tension.

Little correlation between absorbency (as tested according to Standard NZS 2295) and ability to hold condensation on underside of underlay

**ABSORBENCY (as required by Standard NZS 2295) HAS LITTLE RELEVANCE
IN THE MOISTURE BEHAVIOUR OF ROOF UNDERLAYS**

**WATER VAPOUR RESISTANCE HAS AN EFFECT
IN REDUCING CONDENSATION ON THE CLADDING**

NEED FOR MORE RELEVANT “ABSORBENCY” TEST

TEST TO QUANTIFY ABILITY TO HOLD SURFACE MOISTURE

Moisture reaching the upper side of the roof underlay does not percolate through the body of the membrane if the underlay exhibits a high liquid penetration resistance

Moisture forming on the underside of the underlay is mainly held in place by surface tension

The test consists of artificially creating moisture on the underside of a horizontal sample of underlay until drip starts. The maximum amount of condensation before drip starts is considered to be a measure of the surface moisture-holding capabilities of the underlay.

The order of chapters in this report will basically follow the order of this flow chart, with the inclusion of some supplementary chapters. Chapter 2 presents the measured values of some physical properties of a set of roof underlay types in order to give an idea of the range of underlays available. Some of these properties play an important role in the moisture management behaviour of roof underlays. Chapter 3 surveys some field experiment results related to the behaviour of roof underlays under normal Wellington weather conditions. Because during those field experiments little condensation was observed, Chapter 4 illustrates the observations of the behaviour of condensation forming under metallic cladding after that condensation is “artificially” created cooling the roof cladding using dry ice. These observations lead to the study in the laboratory of the very important ability of a roof underlay to cope with condensation directly in contact with the upper side of the membrane. These results are presented in Chapter 5. Chapter 6 describes some modelling efforts that have been put in place to understand the physics of moisture transport in roof underlays. As a result of these modelling efforts it is noted that, under some circumstances, the underlay can behave as a condensation plane and condensation can form on the underside of the membrane. The case of condensation on the underside of the underlay calls for a series of laboratory experiments presented in Chapter 7. Chapter 8 introduces a proposal for a new absorbency test which reflects more closely the behaviour of roof underlays as extrapolated from the different experimental and theoretical results described in this study. To conclude this introduction, a brief survey of the different mechanisms which can give rise to interstitial moisture in roof assemblies is given.

1.1 Mechanisms pertaining to the normal behaviour of a roof

Because the roof is exposed to the elements, it is subjected to continuous and sometimes large variation in temperature, relative humidity (RH) and solar irradiation throughout the day. These variations naturally lead to the formation of condensation on the underside of the roof cladding. If the quantity of condensate is large enough, it can start running down the cladding or dripping.

In the case of metal profiled sheets, favourable conditions for the formation of condensation are found during cold, windless and cloudless nights. When a surface, especially a metallic one, is facing the cloudless sky, it radiates energy away very efficiently and its temperature drops (radiative cooling). If the wind mixes the air around the roof, the temperature of the roof remains close to the temperature of the outside air despite the radiative cooling, because convective coupling to the air dominates over radiative coupling to the cold night sky. However if the wind is absent, convective coupling is very low so that the radiative cooling can bring the temperature of the cladding several degrees below the temperature of the outside air and enhance condensation. This phenomenon is known as “cooling by night sky radiation”.

In the case of an absorbent roof cladding, like old concrete tiles, favourable conditions for the formation of condensation occur when solar radiation heats up a cladding which has absorbed a significant quantity of water. The solar radiation makes most of the water evaporate, but also creates a gradient of vapour pressure which drives a significant fraction (about 10%) of the water deeper into the structure. This phenomenon is known as solar-driven moisture transfer.

1.2 Mechanisms pertaining to the pathological behaviour of a roof

Minor and major failures and design problems can also give rise to interstitial moisture in roof cavities.

If the roof is not perfectly weathertight, wind can drive rain drops into the structure through cracks. In the most serious cases, failures of the integrity of the roof cladding can lead to major leaks.

In certain cases timber which has not been adequately protected and has been exposed to the elements is used to build roofs. Wet timber framing is likely to dry in the first year or two releasing substantial amounts of moisture into the roof space. This case falls under the wide category of “unwanted construction moisture”.

Important quantities of moisture can also find their way into the roof cavity if the roof is covering areas with very moist air and the ceiling is sufficiently permeable.

2. PROPERTIES OF A RANGE OF ROOF UNDERLAYS

2.1 Introduction

Several properties of a range of roof underlays were tested. The properties more likely to affect the moisture management behaviour of roof underlays have been selected. These are:

- Area density: measured in g/m^2 , this represents the mass of 1 m^2 of oven-dry material.
- Water vapour resistance: measured in MNs/g, it indicates the resistance of the material to the passage of water vapour. According to Table 23 of the Compliance Document to the NZ Building Code “External Moisture”, the maximum allowed water vapour resistance is $7 \text{ MN}\cdot\text{s/g}$.
- Water absorbency: measured in g/m^2 , this quantifies the ability of the material to absorb liquid water. According to the Standard NZS 2295, the minimum allowed water absorbency is 150 g/m^2 .
- Liquid penetration resistance: measured with a Pass or Fail, this indicates the resistance of the material to the passage of liquid water. According to the Standard NZS 2295, the minimum allowed liquid penetration resistance is 100 mm.
- Air resistance: measured in $\text{MN}\cdot\text{s/m}^3$, this indicates the resistance of the material to the passage of air. At present, there is no requirement for any level of air resistance.

The properties of 11 building wraps were tested. These building wraps are:

- Wrap A: soft spun-bonded polypropylene non-woven membrane (used for walls).
- Wrap B: spun-bonded polypropylene substrate coated with a polyolefin-copolymer (used for walls and floors).
- Wrap C: microporous water-resistant film sandwiched between two layers of spun-bonded polyolefin (used for roofs).
- Wrap D: spun-bonded high-density polyethylene heat bonded to a polypropylene non-woven sheet (used for roofs).
- Wrap E: diffusion permeable polyolephyne membrane sandwiched between two polypropylene microfiber cover fleeces (used for roofs).
- Wrap F: bituminous Kraft paper (used for roofs).
- Wrap G: coated polyolephyne woven into a sheet form with micropores (used for walls).
- Wrap H: non-woven polypropylene fabric with a water-resistant coating (used for roofs).
- Wrap I: vapour open membrane with metallised low-emissivity surface (for roofs).
- Wrap J: polymer modified with ketone ethylene ester (used for roofs).
- Wrap K: air-tight membrane with metallised low-emissivity surface (used in roofs).

2.2 Area density

Area density was measured gravimetrically. Five $100 \times 100 \text{ mm}$ specimens of each type of underlay were dried at 70°C for 24 hours before being weighed. The drying

procedure was needed to eliminate the bound moisture in the specimens. To some extent, most of the roof underlays are hygroscopic and they tend towards an equilibrium moisture content depending on the RH of the environment they are immersed in Table 1 summarises the results of these measurements.

Table 1: Dry area density of a range of building wraps

Wrap	Area Density (g/m ²)
Wrap A	110
Wrap B	105
Wrap C	265
Wrap D	145
Wrap E	155
Wrap F	370
Wrap G	90
Wrap H	115
Wrap I	135
Wrap J	205
Wrap K	110

2.3 Water vapour resistance

Water vapour resistance was measured using the “Wet Cup Test” described in ASTM E96, Procedure B. A circular specimen of underlay is placed on top of a round container holding distilled water and its edges are sealed with wax. This ensemble is stored in a climate chamber at 20°C and 50% RH for a certain number of days and weighed every 24 hours. The distilled water slowly evaporates and permeates through the specimen of underlay. The rate of mass loss is directly linked with the water vapour resistance of the specimen. Table 2 summarises the results of these measurements.

Table 2: Water vapour resistance of a range of building wraps
(maximum allowed water vapour resistance is 7 MN s/g)

Wrap	Water Vapour Resistance (MN·s/g)
Wrap A	0.15
Wrap B	0.25
Wrap C	0.30
Wrap D	0.40
Wrap E	0.45
Wrap F	0.60
Wrap G	4.25
Wrap H	5.40
Wrap I	24.6
Wrap J	110
Wrap K	3040

2.4 Water absorbency

Water absorbency was measured according to the method described in the standard AS/NZS 4201.6. Five 200 x 200 mm specimens of roof underlay are weighed to obtain their unsoaked weights and then they are immersed in distilled water for 24 hours. After having taken a specimen out of the water, a square 100 x 100 mm is cut out of the centre of it. This square is immersed in the water again for a short instant, and then it is hung for a minute in a vertical position to drain excess water. Finally it is weighed to obtain the soaked weight. From the values of the soaked weight and the unsoaked weight, it is possible to calculate the absorbency. Table 3 summarises the results of these measurements.

**Table 3: Surface absorbency of a range of building wraps
(minimum allowed water absorbency is 150 g/m²)**

Wrap	Surface Absorbency (g/m ²)
Wrap A	140
Wrap B	95
Wrap C	295
Wrap D	80
Wrap E	225
Wrap F	210
Wrap G	0
Wrap H	230
Wrap I	90
Wrap J	50
Wrap K	90

2.5 Liquid penetration resistance

Liquid penetration resistance has been estimated using the method described in the standard AS/NZS 4201.4. A circular specimen of underlay (of an area of at least 25 cm²) is clamped at the bottom of an open cylinder and the edges sealed. The cylinder is kept in upright position with the specimen at the bottom and is put onto a piece of filter paper. The cylinder is then filled with 100 mm of an aqueous solution of distilled water with a dye such as methylene blue. After 24 hours the filter paper is inspected for traces of dye which would signal the passage of liquid water. If no traces of dye are found, the result is Pass otherwise it is Fail. Beyond the requirements of the test, the state of the paper filter was noted: specifically to note if it appeared damp or if its surface had wrinkled. Table 4 summarises the results of these measurements.

2.6 Air resistance

Air resistance was measured according to the methods described in the Standard BS 6538.3 (based on the Standard ISO 6536.5). Some wraps have a labelled side which is quite different from the unlabelled side so two air resistances are measured, with one or the other face on the high pressure side. Table 5 summarises the results of these measurements.

Table 4: Liquid penetration resistance of a range of building wraps

Wrap	Liquid Penetration Resistance	Dampness	Ripples
Wrap A	PASS	Yes	Yes
Wrap B	PASS	No	No
Wrap C	PASS	Yes	Yes
Wrap D	PASS	No	No
Wrap E	PASS	Yes	Yes
Wrap F	PASS	Yes	Yes
Wrap G	FAIL	Yes	Yes
Wrap H	PASS	No	No
Wrap I	PASS	No	No
Wrap J	PASS	No	No
Wrap K	PASS	No	No

Table 5: Air resistance of a range of building wraps. Air resistance is measured with a Gurley apparatus. The description “impermeable” indicates that the air resistance is higher than the maximum value measurable with a Gurley machine. The description “too porous” indicates that the air resistance was lower than the minimum value measurable with a Gurley machine. The description “leaked” indicates that the surface of the wrap does not allow clamping of the Gurley machine in order to conduct an accurate measurement.

Wrap	Air Resistance (MN·s/m ³)	Air Resistance (MN·s/m ³)
	Labelled Side	Unlabelled Side
Wrap A	too porous	too porous
Wrap B	impermeable	0.059
Wrap C	0.041	0.032
Wrap D	leaked	8.43
Wrap E	0.121	3.58
Wrap F	0.567	0.69
Wrap G	0.237	0.243
Wrap H	impermeable	0.046
Wrap I	0.065	3.2
Wrap J	impermeable	impermeable
Wrap K	impermeable	leaked

3. SOME OBSERVED PHENOMENA DURING FIELD EXPERIMENTS

3.1 Introduction

An experimental building was specifically built for this project in order to provide a series of roof specimens exposed to the elements in which to examine the behaviour of roof underlays. The building is rectangular, 15 m long, 7 m wide, has a roof pitch of 15°, sits on a concrete slab and is without internal partitions. The long side of the building is oriented east-west. Five of the roofs are skillion and five are pitched. Each roof specimen has a north-facing slope and a south-facing slope which share a common section of roof ridge and the same type of cladding. Roof specimens can have either of two types of roof claddings: corrugated galvanised steel sheets or old concrete tiles (chosen because of their higher absorbency compared to new ones). These claddings have been chosen because they represent the majority of roof claddings of domestic dwellings in New Zealand.

Of the five roof specimens with a flat ceiling and roof space, three have corrugated galvanised steel sheets and two have concrete tiles. Similarly, of the five roof specimens with sloping ceiling and of skillion type, two are clad with concrete tiles while three are clad with corrugated galvanised steel sheets. However for some experiments some of the corrugated sheets were replaced with trapezoidal profile long metal sheets. The corrugated galvanised steel sheets are unpainted and the concrete tiles deliberately old. Old concrete tiles have lost most of their coating and they are much more absorbent than new ones. They can absorb considerable amounts of moisture (in comparison to their weight) which should enhance the phenomenon of solar-driven moisture.

3.2 Evidence of night sky radiative cooling

Night sky radiative cooling is the phenomenon by which horizontal or sloping surfaces facing the sky during the night can cool below the temperature of the outside air. Especially during cloudless and still nights the sky behaves as a black body at a temperature well below the outside air temperature. Empirical relationships show, for example, that when the outside air temperature is 5°C the night sky behaves as a black body at around minus 8°C, and when it is 0°C as a black body at around minus 14°C. As a consequence surfaces facing the sky radiate heat away. If there is no or little wind, the surface may quite easily cool several degrees below the ambient temperature, and often below the ambient dewpoint. If there is even a moderate air movement, convective heat transfer quickly dominates over radiative cooling and the temperature of the surface equilibrates with the temperature of the outdoor air.

Figure 1 shows an example of night sky radiative cooling. During the night between 24 June and 25 June 2008, the sky was cloudless and the outside temperature fell to around 0°C for part of the night. At the same time the wind was nearly absent. The right conditions for night sky radiative cooling were all present and indeed the temperature of the cladding plummeted to around minus 5°C!

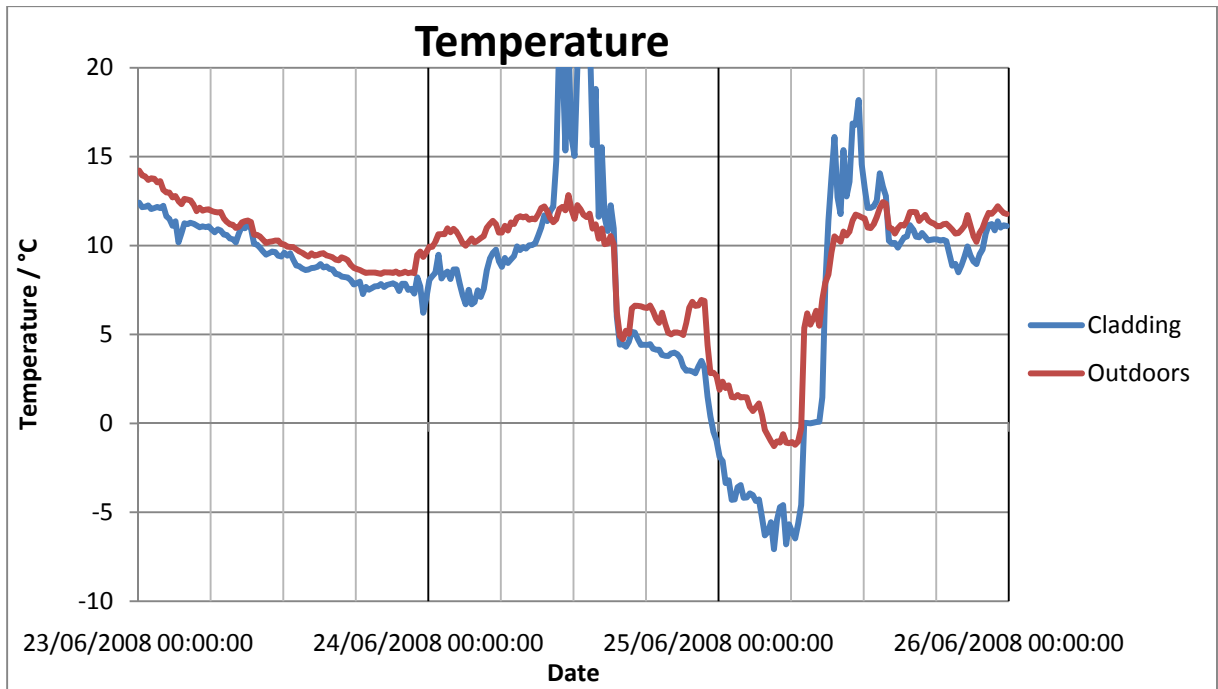


Figure 1: Example of night sky radiative cooling during cloudless and still nights when the temperature of the cladding can significantly drop below ambient temperature

Gravimetric measurements during night sky radiative cooling are very instructive in monitoring the wetting and drying of the roof underlay during an episode of night sky radiative cooling. The monitoring of the underlay is done by means of a so-called “condensation apparatus”; at regular time intervals, a small removable part of the cladding is taken off and a small removable part of the roof underlay is weighed. The condensation apparatus is shown in Figure 2 for metal roofs and in Figure 3 for roofs with concrete tiles.

Figure 4 shows the temperature of the outdoor air and the temperature of a metallic cladding surface. The night between 6 September and 7 September 2008 was marked by an episode of night sky radiative cooling lasting more than 12 hours and bringing the temperature of the cladding to sub-zero values for most of the night. The wind speed was initially small and then it became moderate. This only marginally reduced the effectiveness of the radiative cooling during the second half of the night. As a consequence of the sub-zero temperature of both the metallic cladding and of the concrete tiles, all exposed surfaces were covered by a thin layer of ice from around 8pm through to around 6am of the following day. The layer of ice grew thicker during the night.

During the regular weighing of the underlay, a visual inspection of the underside of the cladding was carried over in order to observe if droplets of condensate were forming. Quite surprisingly, no evident condensation was observed.

Figure 5 presents the results of the weighing of the roof underlay. Weight increases and decreases are interpreted as absorption and desorption of moisture by the square sample of underlay forming the condensation apparatus. Instead of reporting the weights, the graph shows values of moisture content (the mass of water bound to the specimen or sitting at its surface is expressed as a fraction of the dry weight of the specimen itself).

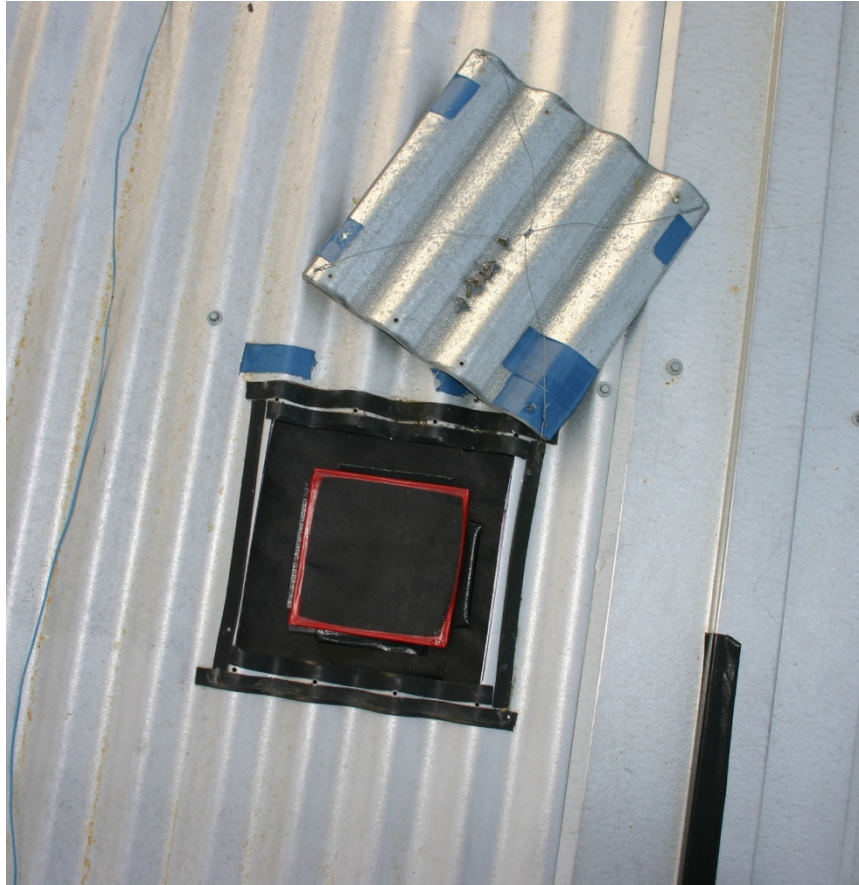


Figure 2: Picture of the condensation apparatus for roofs clad with metal sheets



Figure 3: Picture of the condensation apparatus for roofs clad with tiles

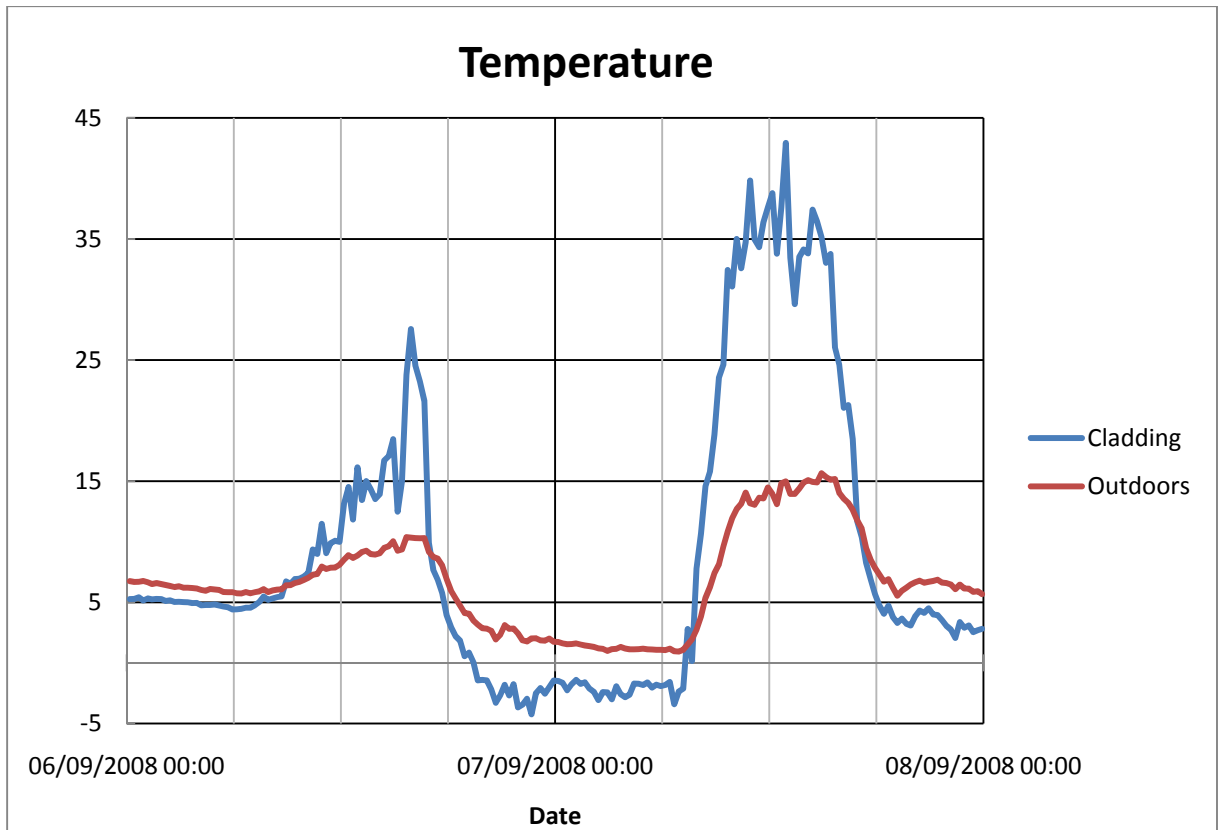


Figure 4: Another example of night sky radiative cooling (the corresponding gravimetric measurements are presented in Figure 5)

Two types of roof underlays were considered: a traditional paper-based product (Wrap F) and a trilaminate synthetic product (Wrap C). These roof underlays were installed both in skillion and pitched roof specimens and with both metallic cladding and concrete tiles. Due to the different hygroscopic characteristics of the two membranes, their moisture content levels are quite different. Wrap F is very hygroscopic while Wrap C is only moderately hygroscopic.

The behaviour of the paper-based underlay seems to depend on the type of roof (skillion or pitch), but much less on the type of cladding of the roof (metallic cladding or concrete tiles). In the case of the skillion roof, the moisture content rises quite considerably, from around 10% to over 20%, while in the case of the pitch roof the increase is much smaller, from around 10% to around 13%. Having a metallic cladding or concrete tiles does not seem to have a major effect except a slightly greater rise in moisture content in the case of metallic cladding.

The behaviour of the trilaminate synthetic product is less pronounced as the material is only moderately hygroscopic. In the case of the skillion roof, there are moisture content increases of 3-5% while in the case of pitch roof it stays roughly constant.

It has been noted that on the underside of the cladding no droplets of condensate were observed. That seems to exclude the belief that the increase of moisture content in the roof underlay was due to droplets of water dripping from the underside of the cladding onto the roof underlay. The variation in moisture content should then mainly be attributed to the hygroscopic behaviour of the underlays and to surface condensation. The cooling of the cladding makes the RH in the cavity between underlay and cladding increase and, as a consequence, the moisture content increases following the sorption curve of the material. Once an RH of 100 % is reached condensation could create a

film of unbound water at the surface of the underlay that would lead to a further weight increase.

The moisture content reached at its highest around 24% for Wrap F (paper-based) and around 5% for Wrap C (synthetic trilaminate). Comparing these values with the sorption curves for Wrap F and Wrap C presented in Figure 36, we can observe that in both cases the moisture content remained in the hygroscopic region, below or near saturation. This would point to the fact that there was no unbound water condensing at any time on the surface of the underlay.

The difference in behaviour of the paper-based underlay, and to a minor extent of the synthetic underlay depending on the type of roof (pitch or skillion), could hint to the role of ventilation. In a skillion roof two rather small cavities separate the underlay from the underside of the cladding and from the top of the insulation. In a pitch roof there is a small cavity between the underlay and the underside of the cladding, but a much larger space under the underlay (the roof space). Ventilation in the roof space probably inhibits the absorption of moisture by the underlay.

Further investigations and modelling are needed to fully understand the dynamics of absorption and release of moisture by the underlay. But the most notable observation is that even under prolonged conditions of night sky radiative cooling, no evidence of dripping condensation from the underside of the cladding onto the underlay was detected in the Wellington climate that the roofs were exposed to.

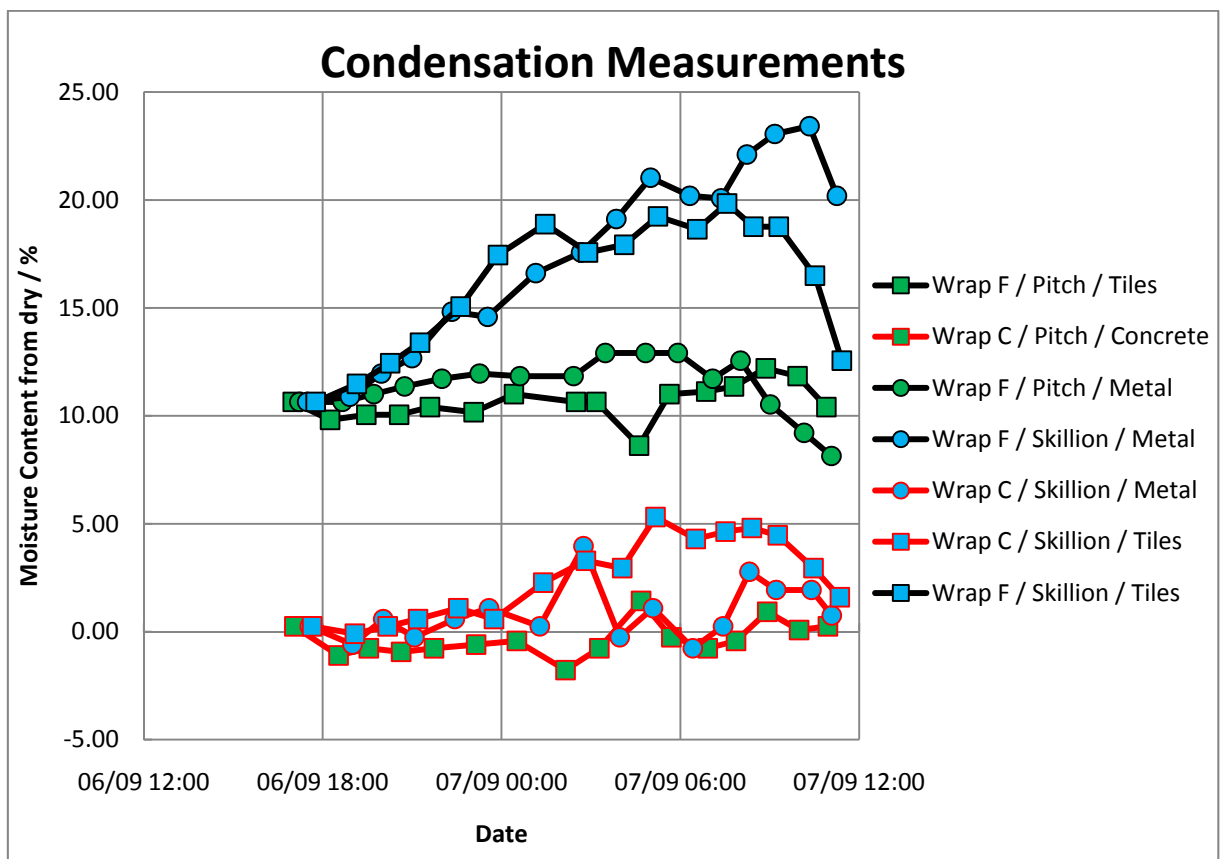


Figure 5: Gravimetric condensation measurements during the night sky radiative cooling presented in Figure 4. The weight of the section of underlay (part of the condensation apparatus) was measured at regular intervals during the event, then it was converted to moisture content using the area density of the dry material reported in Table 1.

3.3 Negative observation of solar-driven moisture

The phenomenon of solar-driven moisture is one by which moisture is driven inside a structure by solar radiation. In roofs, the phenomenon is only possible with absorbent claddings like fibre-cement or old concrete tiles. During a rain event, tiles can absorb a considerable portion of their weight in water. When solar radiation shines on a wet tile, it evaporates most of the absorbed water to the outdoors, but also drives a fraction of the absorbed water into the cavity above the underlay. The temperature difference between the side of the tile exposed to the solar radiation and the unexposed one creates a large vapour pressure gradient that drives a fraction of the absorbed water inside while the majority of the water evaporates.

Some experiments have been done in order to estimate the importance of this phenomenon. In order to possibly enhance the effect of solar-driven moisture, we artificially watered the roof specimens with concrete tiles during a night preceding a sunny day. The watering was done using a hose pipe in the shape of a ribbon with many little holes along its length in order to achieve a more or less even irrigation along the width and the slope of the roof specimens. The watering of the roof specimens was done at night in order to avoid evaporation and solar gain. In the morning, the water was turned off and measurements using the condensation apparatus were made. The weight of the modified tile and of the weight of the 150 x 150 mm square of underlay were monitored regularly for a period of a few hours. The aim was to detect a rise in moisture content of the underlay due to moisture absorbed by the tiles driven towards the inside of the structure. The tile and the underlay were weighed before starting watering the roof, and Figure 7 show their weight increase after the watering. The underlay used was Wrap F, a paper-based roof underlay.

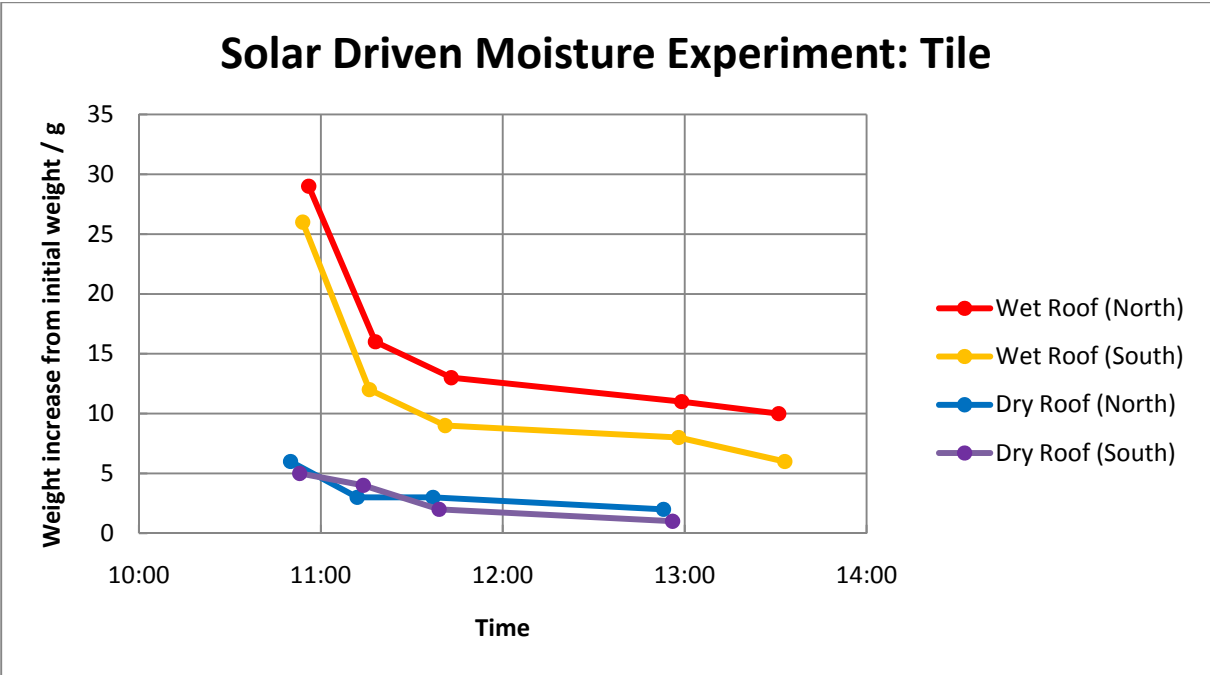


Figure 6: Difference between the weight of the modified tile of the condensation apparatus after watering the roof specimen and its weight just before starting watering the roof (called “initial weight”). One roof specimen was watered during more than 18 hours (simulating the equivalent of 100 mm of rain) and one was left dry. The graph represents the evolution of the weights after the watering was stopped and while solar radiation dried the roof

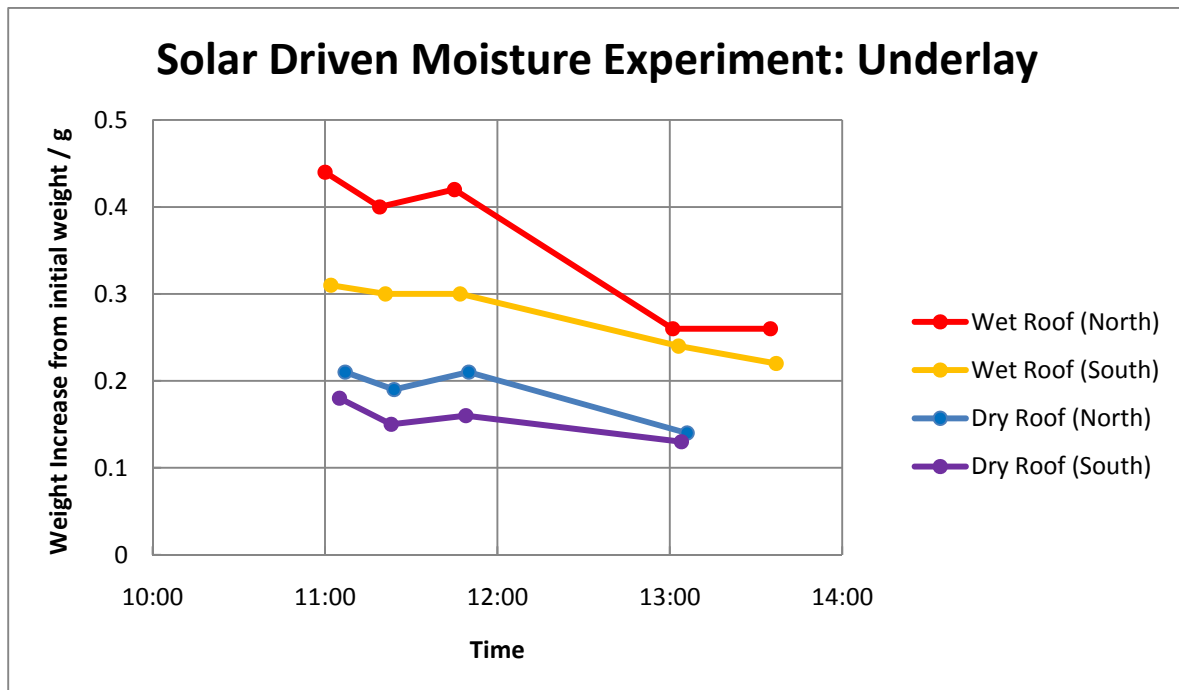


Figure 7: Difference between the weight of the section of underlay of the condensation apparatus after watering the roof specimen and its weight just before starting watering the roof (called “initial weight”). One roof specimen was watered during more than 18 hours (simulating the equivalent of 100 mm of rain) and one was left dry

The graph represents the evolution of the weights after the watering was stopped and while solar radiation dried the roof.

The weight of the square of underlay and of the modified tile of the condensation apparatus were taken before starting watering the roof tiles and then at regular intervals after the hose was turned off. No measurement was made while the water was running down the slopes of the roof specimens.

The tiles of the roof specimens which were not watered show a slight weight increase compared to the weight the day before, followed by a decrease. The initial weight increase is probably due to spray carried from the neighbouring watered roof specimen. In comparison, the tiles of the roof specimens which were watered show a far more pronounced weight increase compared to the weight the day before, because of absorption of water. Most of the absorbed water then quickly evaporates.

The weight of the 150 x 150 mm square of roof underlays exhibits an initial weight increase compared to the weight the previous day. The weight of the underlay in the roof specimens which were not watered decreased only slightly during the measurement period. The decrease is more pronounced for the square of underlay in the roof specimen which was watered. Figure 8 shows the behaviour of the RH in the cavity between underlay and cladding of the two roof specimens. From around 9am the RH starts decreasing due to the effect of the solar radiation shining on the roof specimen which was not watered. From around 11am to 2pm, the period covered by the measurements, the RH in this roof specimen stayed approximately constant and that agrees with the fact that the weight of the underlay only changed marginally. In the roof specimen which was watered, the RH only started decreasing at around 11am, when the watering of the roof stopped, and continued during the period covered by the measurements. This is an agreement with the decrease in weight of the underlay.

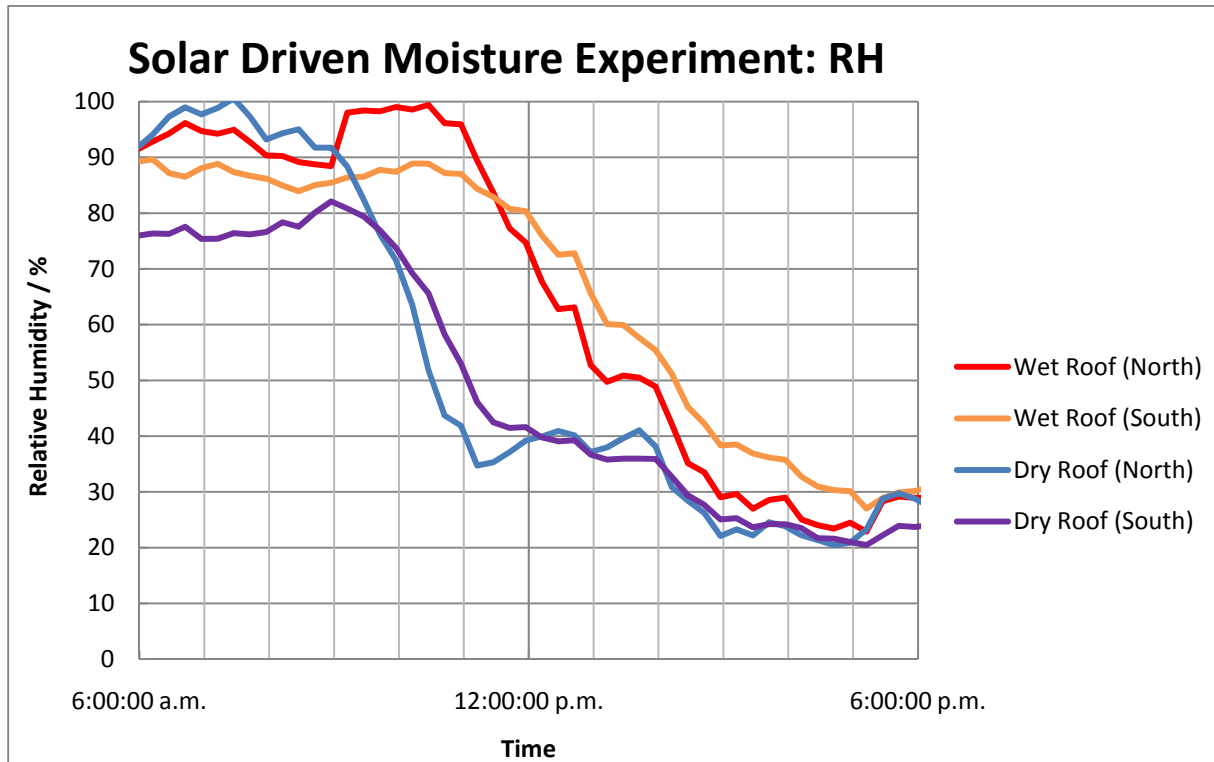


Figure 8: Evolution of the relative humidity in the cavity between underlay and cladding during the final phase of the watering and during the drying of the roof specimens. One roof specimen was watered for 18 hours simulating the equivalent of 100 mm of rain and one was left dry. The sun rose at around 6.30am and the watering was stopped at around 11am

If the phenomenon of solar-driven moisture was significant the behaviour of RH and of the weight of the underlay should be quite different. If solar radiation drove detectable quantities of moisture into the structure while the sun was shining on a wet absorbent cladding, the RH should remain at high levels for a certain period of time after the watering of the roof specimen has stopped. Instead the RH starts dropping as soon as the watering of the roof ends. Between 9am and 11am the RH of the north slope of the roof specimen which was kept wet rose sharply. That could be an indication of the presence of some solar-driven moisture when the water was still continuously running down the slope of the roof, but the sun had already risen and was heating up the concrete tiles.

3.4 CONCLUSION

Even if the phenomenon of solar-driven moisture was active, its effect on the hygrothermal environment seems very marginal. Visual inspection of the underlay did not show any evidence of dripping condensation from the underside of the concrete tiles.

4. DRY ICE RESULTS

4.1 Introduction

Little condensation on the underside of the cladding was observed during the field experiments described in Chapter 3. Similarly, no evident sign of drip onto the upper side of the underlay was clearly detected.

An artificial situation was set up to achieve more extreme conditions in the field in order to create sufficient condensation to be able to observe how the underlay behaves. To create condensation on the underside of the metal cladding of a roof specimen of the test house, the external surface of the roof cladding was covered in dry ice pellets. These pellets (in the shape of small cylinders 2-3 cm long) are made of frozen CO₂ and they sublime at temperatures around -80 °C. Dry ice was chosen because it is readily available and it sublimates instead of melting. The dry ice pellets were placed on a plastic mesh which was fixed to a metallic frame as large as the surface of the roof specimen as shown in Figure 9.

The plastic mesh kept the dry ice pellet at 1-2 cm from the metal cladding and prevented the pellets from rolling down the slope of the roof. Thick polystyrene blocks were placed all around the perimeter of the metal frame as shown in Figure 10, and thick polystyrene panels were placed on top of those so to cover the plastic mesh and the dry ice pellets. The polystyrene blocks and panels created a sort of insulated cavity above and around the slope of the roof and around the metallic frame with the plastic mesh supporting the dry ice pellet. Due to the sublimation of the dry ice pellets, the air inside this temporary cavity was cooled down to a temperature of the order of -50 °C or more. In turn the very cold air entrained the fast cooling of the roof to a temperature of -30 °C or more. This situation could be maintained for around 30-40 minutes while the dry ice pellet sublimated. After that, the polystyrene blocks and panels were quickly removed, together with the metallic frame supporting the plastic mesh and the eventual residual dry ice pellets.

During the cooling phase, the underside of the metallic roof cladding is quickly covered by a thin layer of ice which gets thicker and thicker. Once the dry ice is removed, the temperature rapidly rises and the layer of ice quickly melts creating significant quantities of condensation on the underside of the cladding. Some results and observations gathered from these “dry ice” experiments are presented in the next section.



Figure 9: Metallic frame used to support the dry ice pellets in the dry ice experiment.



Figure 10: Polystyrene enclosure surrounding the metallic frame during the dry ice experiment. During the experiment thick polystyrene sheets sit on the polystyrene enclosure and cover the metallic frame in order to create an insulated cavity above the metal cladding.

4.2 Results and observations of the dry ice experiments.

During the cooling phase and after the dry ice pellets were removed, the underside of the underlay was continuously monitored by means of a boroscope. This is an optic fibre video camera which allows imaging location in very confined spaces. In a very schematic way, a boroscope has a high quality miniature lens which collects the light that is then sent down an optical fibre towards the recording unit. The optical fibre is encased in a sturdy, flexible and slim sheathing to give manoeuvrability and protection to the fibre itself.

The boroscope was introduced into the cavity between underlay and a corrugation of the profiled metallic cladding using the natural opening which exists at the level of the eaves of the roof specimen. A short focal right angle lens was used to provide an image of the underside of the cladding at more or less midway between eaves and ridge of a slope of the roof specimen.

The series of pictures in Figure 11 to Figure 17 show the evolution of the surface of the underside of the metal cladding during the duration of the dry ice experiment.

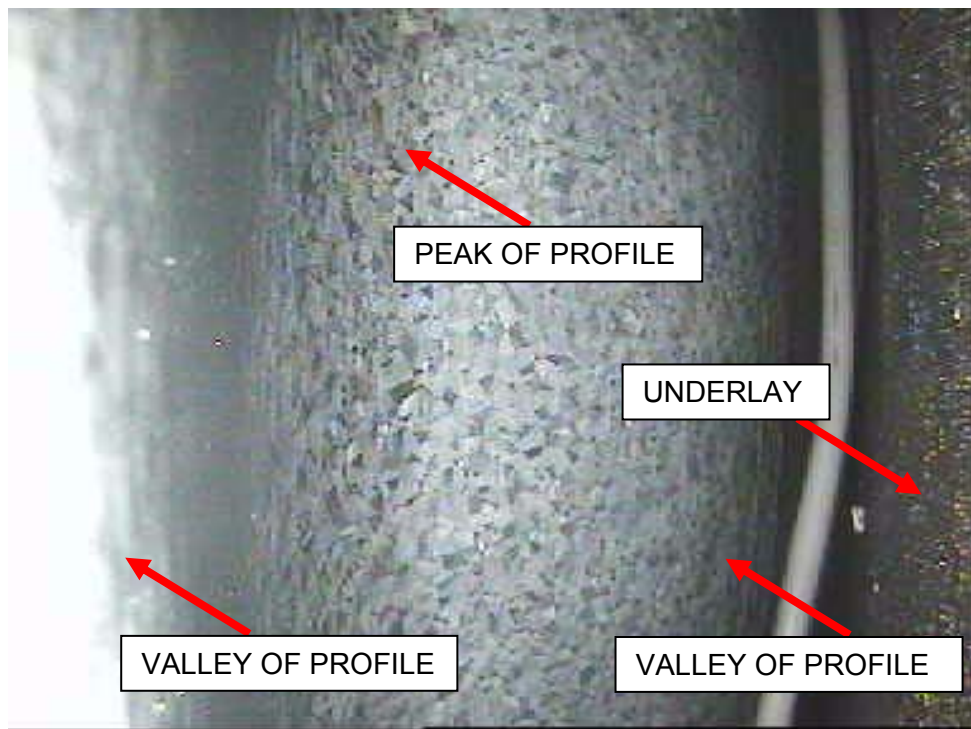
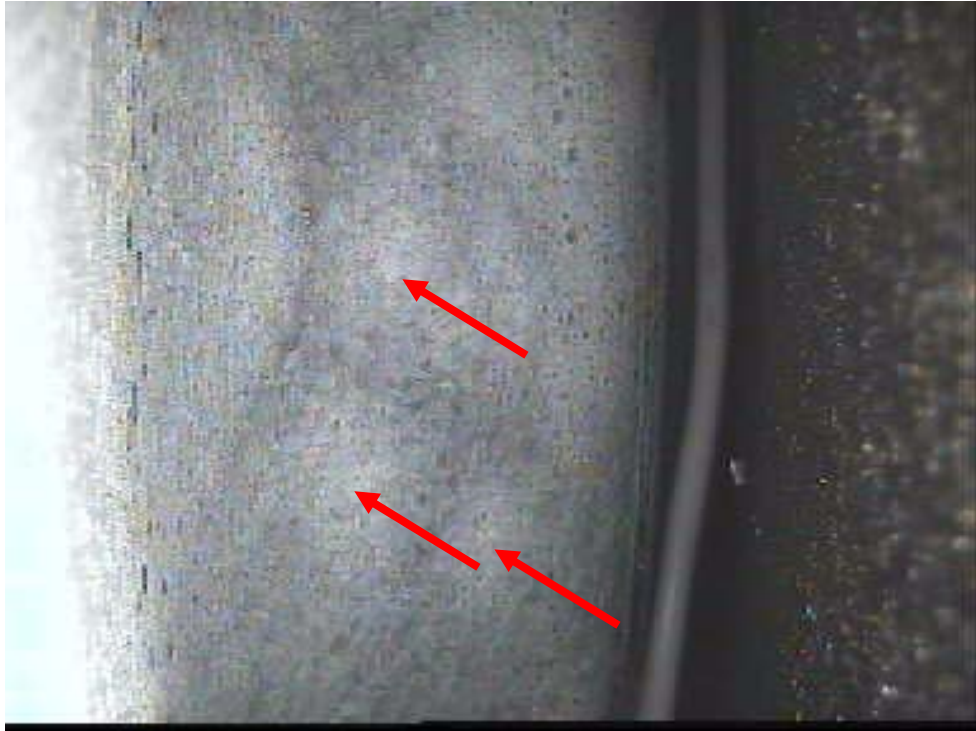


Figure 11: Initial condition of the cavity between corrugated metal cladding and underlay. The picture was taken using a boroscope and the point of view is looking across the short length of the cavity



**Figure 12: Condition of the cavity 10-15 minutes after the start of the dry ice experiment.
The underside of the metal cladding is covered by a thin layer of frost**



**Figure 13: Condition of the cavity 30-40 minutes after the start of the dry ice experiment.
The underside of the metal cladding is covered by a thick layer of frost**



Figure 14: After removing the dry ice, the layer of frost starts to melt nearly immediately

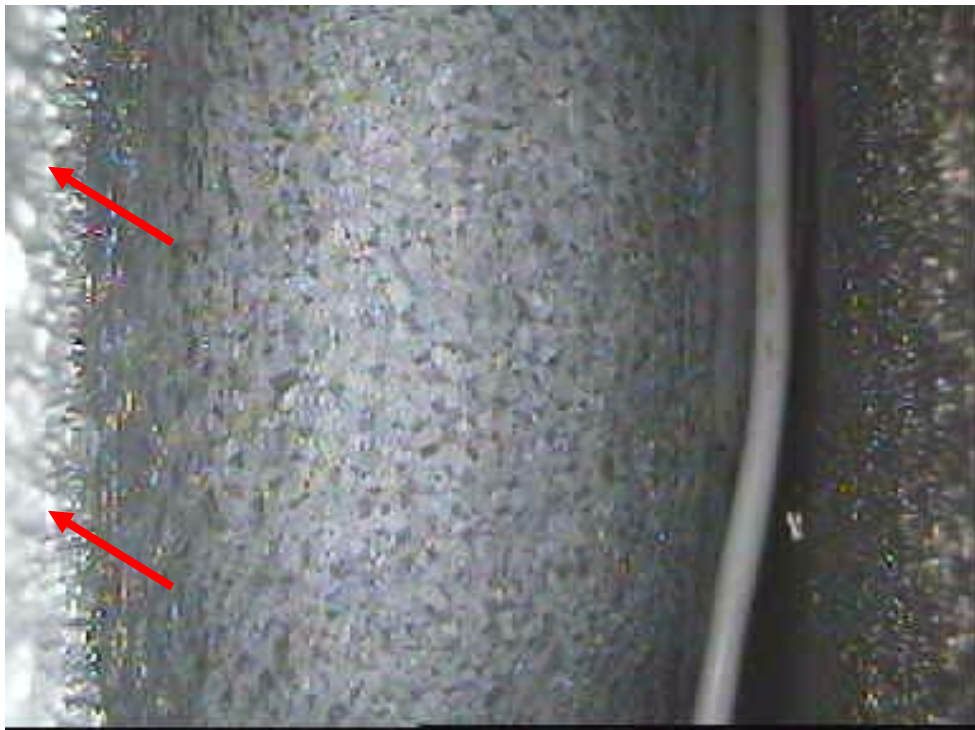


Figure 15: After the layer of ice has quickly melted, the surface of the metal is covered by fine water drops

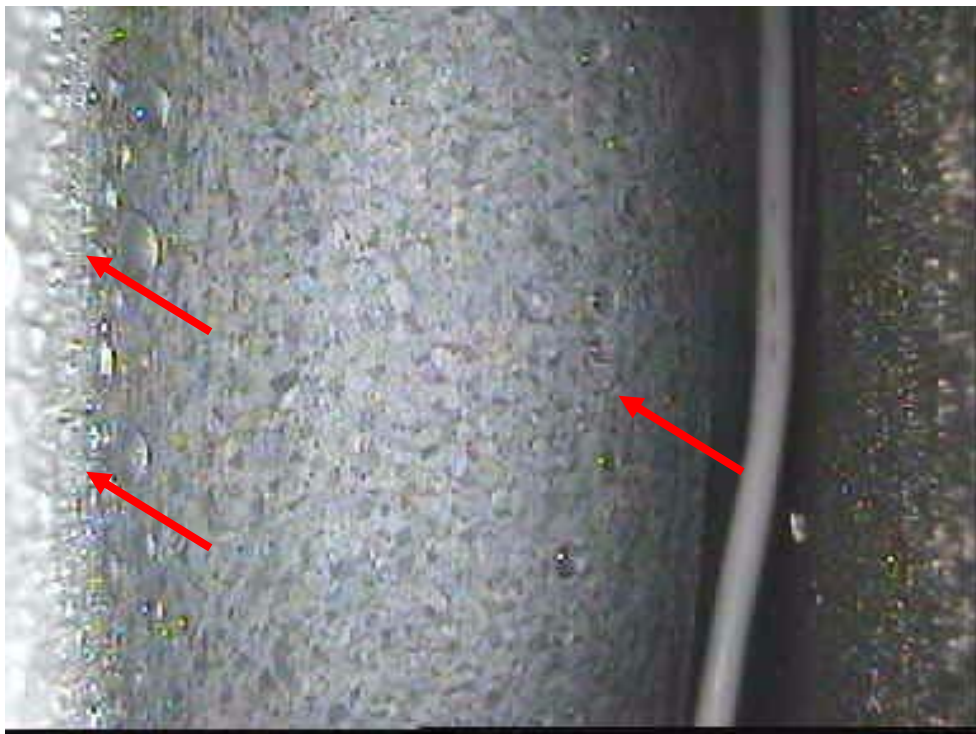


Figure 16:The fine water droplets soon coalescent into big drops, especially near the lower parts of the metal profile



Figure 17: Condensation accumulates near the valleys of the corrugated metal profile

In Figure 11 we can see the surface of the metal as it is before starting the experiment. This picture and those in Figure 12 to Figure 16 are all taken from the same point of view. Normally, in a roof assembly, going from bottom to top, we find the roof underlay surmounted by the corrugation of the metal profile. In the picture, the underlay is on the right and we can see two valleys (one clearly and the other out of focus because too close to the lens) and one ridge. In Figure 11 the many tiny domains that form the surface of the metal shine under the light of the boroscope. A few minutes after putting the dry ice, a thin layer of ice starts forming on the metallic surface as seen in Figure 12. After around half an hour of cooling, the layer of ice is sufficiently thick and uniform to hide all the tiny domains that constitute the surface of the metal as shown in Figure 13. Shortly after the polystyrene blocks and panels and the metallic frame are removed, the layer of ice starts to melt as seen in Figure 14. The melting ice leaves behind tiny droplets which are lit by the grazing light of the boroscope in Figure 15. Droplets were present also on the side which was directly in front of the camera but cannot be easily seen. Those tiny droplets soon coalesce into big droplets which then tend to slide towards the valleys of the metal profile as seen in Figure 16.

4.3 Conclusions

From the series of pictures it can be inferred that when condensation does form, it begins as small water droplets which then coalesce into big droplets. These water droplets do not drip but stay localised by the action of surface tension or slide towards the lowest regions of the metal profile. Condensation thus ends up sitting in contact with the upper surface of the underlay under the lowest regions of the metal profile, without evident signs of dripping and limited evidence of draining down the underlay.

The underlay has to be able to prevent the water from being transferred to the layers underneath. The dry ice experiments have shown that condensation accumulates at the interface between metal cladding and underlay and it sits there. Two properties of the underlay deal with retaining water which forms or accumulates on the upper side of the underlay: liquid penetration resistance and absorbency. As presented in Chapter 2, liquid penetration resistance characterises the ability of the underlay to withstand for 24 hours a 100 mm column of water without having water seeping through to the other side. Absorbency is the ability to retain water in the body of the underlay. Experiments were conducted in order to study the relative importance of these two properties in managing moisture originating above the underlay laboratory. These experiments are presented in the following chapter.

5. AN EXPERIMENT TO EXAMINE STUDY UPPER SURFACE LIQUID

5.1 Introduction

The dry ice experiments show that condensation accumulates at the interface between the metal cladding and underlay. Liquid water can also reach the upper side of the underlay in the case of wind-driven rain that makes its way through minor defects of the roof cladding or in the case of major leaks.

A roof underlay can absorb the liquid moisture, deflect it or both. In order to study the relative importance of these mechanisms and their possible interplay, an experiment was set up in a climate chamber. Its aim is to study what happens to water droplets that accumulate at the surface of the underlay, especially those transferred to the underlay where it may touch the low point of the cladding where condensation accumulates. This experiment also covers the case of small water leaks from the roof cladding. Small leaks generate the accumulation of liquid water on the surface of the underlay, and sometimes in vastly greater quantity than condensation.

5.2 Set-up of upper surface liquid experiment

A 350 x 350 mm square sample of roof underlay is clamped to a hollow square metallic frame which can be tilted to a desired angle as shown in Figure 18. This ensemble underlay plus metallic frame simulates an underlay installed on a sloping roof. The ensemble is kept in a climate chamber at cool temperatures, around 5 °C, and relatively high RH, around 90%. Those conditions are the most extreme that can be achieved with the compact climate chamber available, but they adequately represent the situation of a cool night.

In order to simulate the accumulation of liquid water on the upper side of the underlay, a manifold of small plastic (Figure 19) tubes is placed near the upper edge of the underlay. The manifold is then connected to a series of small plastic tubes where distilled water is fed by using a peristaltic pump. This pump can achieve very low flow rates. In the dripping experiment, a rate of 600 ml/hour is used which equates to 3.5 litres/(m² hour). This is one of the lowest rates achievable with the peristaltic pump used. This rate is representative of a major leak in the roof cladding. The results obtained in this case will be also valid for much lower moisture accumulation.

The dripping experiment is carried out in different phases. In order to allow the underlay reaching the hygroscopic equilibrium, the 400 x 400 mm square underlay specimen is clamped to the metal frame and left for 24 hours in the climate chamber before starting the experiment. Also a 200 x 200 mm square sample of underlay is conditioned in the chamber at the same time, for reasons explained later. The experiment then consists of switching on the peristaltic pump, running distilled water over the upper side of the specimen and observing at regular intervals the behaviour of the water droplets. Due to the configuration of the manifold and the low flow rate, the water droplets are generated in contact with the surface of the underlay and they grow at a very slow pace. This is an approximation of what has been observed in the field concerning the accumulation of moisture. The water is left running for five hours and the chamber is opened regularly to inspect the surface of the underlay.

The 200 x 200 mm square sample of underlay is taken from the chamber and weighed at the beginning of the experiment. Soon after, it is put back into the chamber and left there during the five hours of the experiment. Care is paid not to have this underlay specimen coming into contact with any of the water running in the chamber. After the end of the experiment, the 200 x 200 mm sample is weighed again. The difference in weight between the end and beginning of the experiment allows an estimation of the amount of moisture the underlay clamped on the metal frame would have gained if it

had simply stayed in the climate chamber for five hours without any liquid water running on its surface.

At the end of the five hours a 200 x 200 mm square is cut from the centre of the 400mm x 400mm underlay sample clamped on the metallic frame and weighed. Surface water is wiped off the surface and the 200 x 200 mm square sample is weighed again. This gives an indication of how much water has been absorbed in the body compared to the one sitting at the surface.

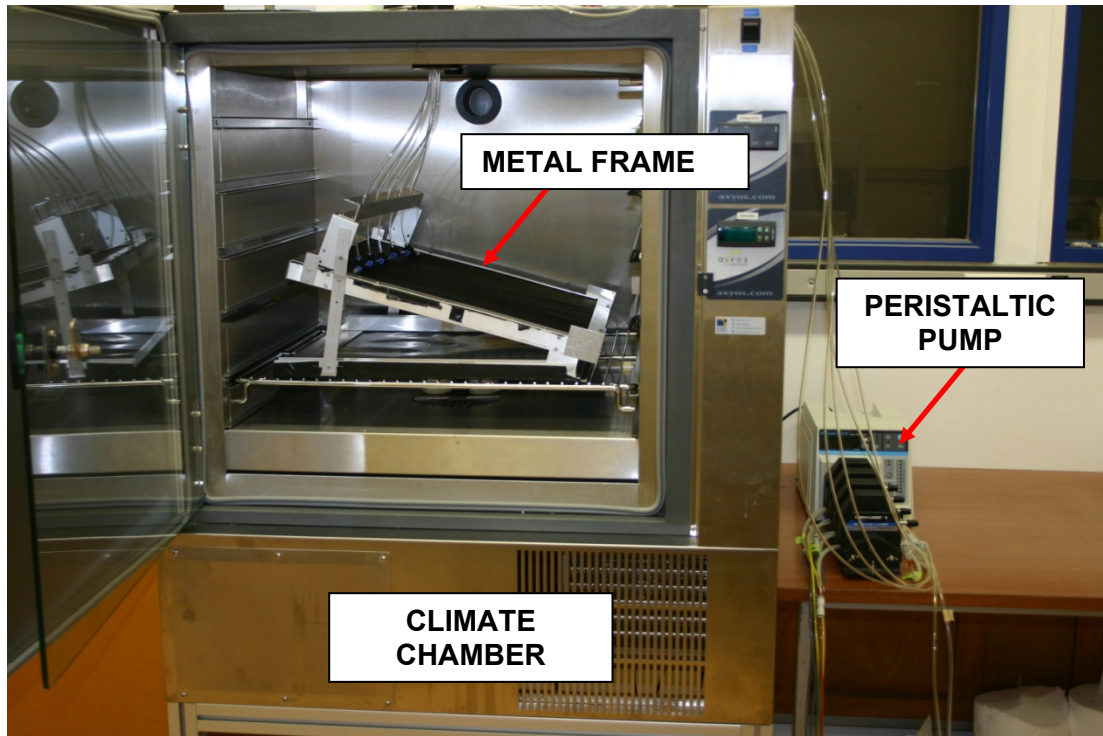


Figure 18: Set-up for the upper surface liquid experiment. An underlay specimen is mounted on a sloping metallic frame which is placed in a climate chamber. A set of small plastic tubes connected to a peristaltic pump provide a source of condensation forming in contact to the upper surface of the underlay

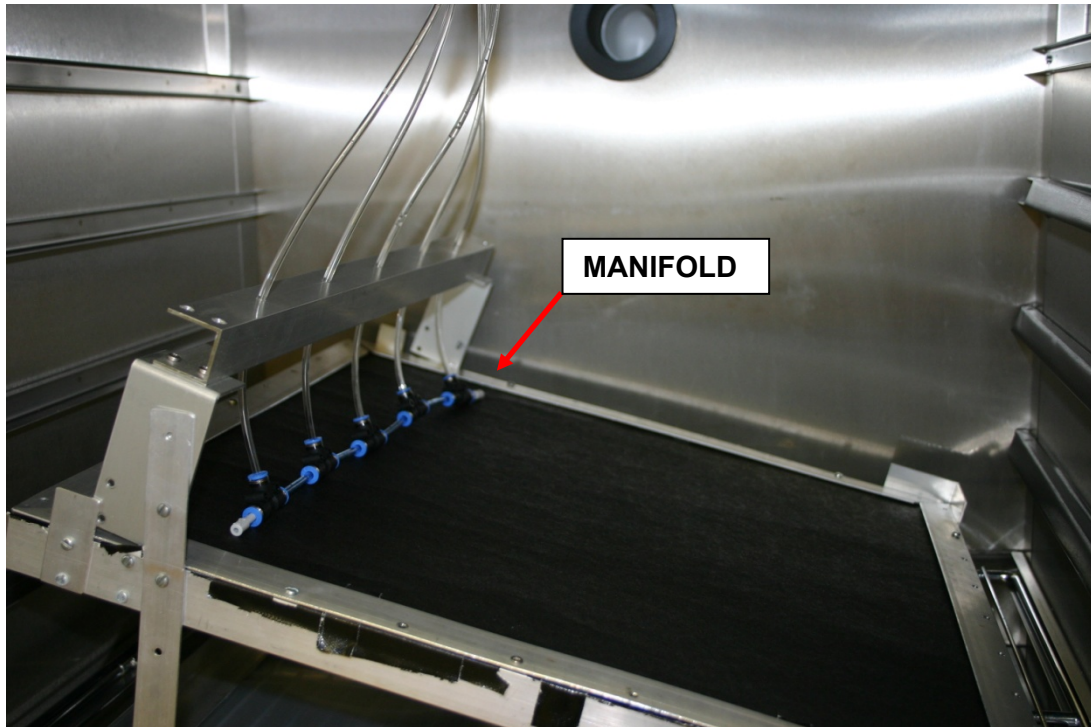


Figure 19: Detail of the manifold which artificially creates contact liquid on the top edge of the underlay specimen

5.3 Results of the upper surface liquid experiment

As a general comment, all roof underlays tested in the way described above show a similar behaviour. Water droplets run down the underlays without being significantly absorbed on their way downwards. There is little difference between the roof underlays which are considered “very absorbent” or “little absorbent” according to the absorbency test described in the Standard AS/NZS 4201.6. It could have been expected that “absorbent” underlays would absorb the tiny water droplets coming from the manifold installed at the top edge of the underlay sample. But all the underlays tested exhibited the same hydrophobic behaviour.

Another important observation is that even after five hours of heavy watering, no sign of water percolating through the body of the underlay towards the underside of the membrane was observed. The underside of all underlays tested stayed perfectly dry.

Some quantitative, although quite imprecise, measurements were taken, as explained above. For Wrap F, the initial weight of the control sample (the one not watered but kept in the climate chamber) was 16.88g and the final weight was 17.38g. It can be inferred that Wrap F would increase its weight by 12g/m² if no watering occurs. Being Wrap F, a paper-based underlay, it has a well-pronounced sorption curve. The observed weight increase is due to the fact that the RH increased in the climate chamber during the duration of the experiment. The water which runs on top of the underlay and drips off the bottom edge of the metal frame is collected in a tray which remains in the climate chamber. This water being kept in a confined space makes the RH rise in the climate chamber. The weight of the 200 x 200 mm cut from the sample which was watered was 19.98g. After the water droplets at the surface of the sample were wiped off, the weight was 18.67g. This last weight is to be compared with the final weight of 17.38g for the control sample. The watered sample is slightly heavier than the control sample. We can interpret the excess as water that has been absorbed into the body of the underlay, whose amount is around 30g/m². This amount should be

compared with the value of 210 g/m² obtained doing the traditional absorbency test described in the Standard AS/NZS 4201.6.

For Wrap D, the initial and final weights of the 200 x 200 mm control sample were 6.06g and 6.07g. Wrap D has a flat hygroscopic curve, so it does not adsorb any moisture in the hygroscopic region. This explains why the control sample did not change weight. The 200 x 200 mm sample cut out the centre of the underlay which was clamped on the metallic frame and weighed 6.50g at the end of the five hours. After having wiped off the surface water, the weight was 6.09g. In the case of this membrane, practically no liquid moisture was stored in the body of the underlay. This value should be compared with the value of 80 g/m² given by the traditional absorbency test.

5.4 Conclusions

Several underlays with different properties were tested using the dripping experiment set-up. All underlays behaved in a similar manner; most of the water droplets forming at the surface of the upper side of the underlay are held on the surface and eventually run down the membrane. In the case of paper-based underlays, a fraction of the water is held in the body of the membrane. On the contrary, in the case of synthetic underlays, very little water is held in the body of the membrane. This contrasts with the water absorbency measured with the standard test described in AS/NZS 4201.6 and that is required to be at least 150 g/m² by the Standard NZS 2295 in order for an underlay to be acceptable as roof underlay. The ordinary AS/NZS 4201.6 test does not seem to represent what is happening in the case of liquid arriving on the upper side of the underlay. What seems important is the ability of the underlay to prevent the water from seeping through the membrane.

This behaviour is better captured by a property other than the traditional absorbency, viz. the liquid penetration resistance. All roof underlays are required to pass the liquid penetration resistance test described in Chapter 2. As stated previously this test consists of having a sealed cylinder filled with 100 mm of dyed water sitting on top of an underlay specimen for 24 hours. At the same time a white paper filter is placed under the underlay sample. If, after the 24 hours, no trace of dye is seen on the paper filter, the underlay passes the test. All roof underlays which have been subjected to the dripping test pass the liquid penetration test, but not all of them have a value of absorbency (in the AS/NZS 4201.6 sense) of 150 g/m². Despite not being considered sufficiently absorbent, they all perform equally well in the task of deflecting water from the wood framing and insulation.

In this case, the water penetration resistance seems to be the key property with the traditional absorbency only playing a marginal role.

6. AN ANALYTICAL MODEL TO EXAMINE THE EFFECT OF UNDERLAYS ON CONDENSATION RATES UNDER METAL ROOFS

6.1 Model description

The roof system is modelled with three nodes, viz. the small cavity between the underlay and the roof, the underlay itself and the large cavity below the underlay, and four moisture sources, viz. indoors, outdoors and the condensation under the roof (see Figure 20 and Figure 21). Moisture from indoors and outdoors is transported by both air movement and vapour diffusion. So if Q is the vapour transported we have, using the ideal gas equation

$$\begin{aligned} Q &= VF(c_a - c_b) + \frac{A(p_a - p_b)}{r} \\ &= \left(\frac{VFW}{RT} + \frac{A}{r} \right) (p_a - p_b) \end{aligned} \quad (1)$$

where small density changes in the air, as it moves into regions with different temperatures, are ignored. We can define an effective vapour resistance r , and its inverse h , by equating vapour flow through the effective resistance to the total flow given in equation (1) as follows:

$$\frac{A(p_a - p_b)}{r} \equiv \left(\frac{VFW}{RT} + \frac{A}{r} \right) (p_a - p_b)$$

that is

$$\frac{1}{r} = h \equiv \left(\frac{VFW}{ART} + \frac{1}{r} \right) \quad (2)$$

6.1.1 High and low hygroscopic papers

There is an important difference between hygroscopic Kraft paper underlays and synthetic underlays which are usually of low hygroscopy. If condensation is taking place onto the lower surface of the underlay and if it is hygroscopic and absorbent (e.g. Kraft paper), the condensation is absorbed quickly and distributes itself through the width of the paper with liquid moisture appearing on the top. However, if the underlay is synthetic it will often be multi-, often three-, layered with the central layer being the vapour resistive part of the underlay. Importantly condensation is not absorbed into these papers and does not move through to the upper surface, but is held as visible drops under the surface by capillary forces, particularly if that surface is dimpled.

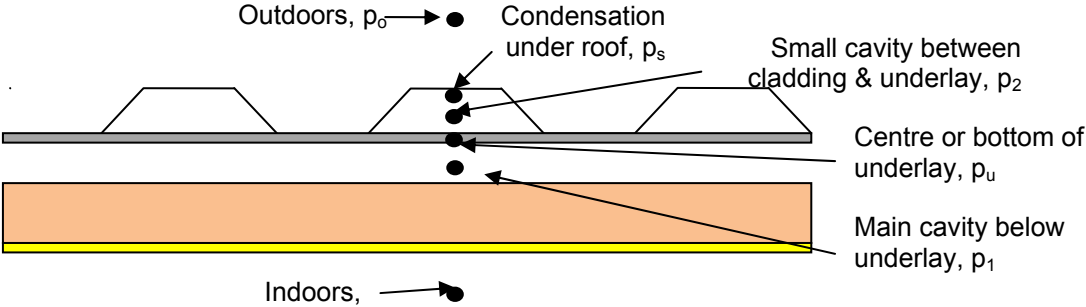
This difference reflects into different expressions for the size of h_{1u} and h_{2u} in the model of Figure 21. For Kraft-type underlays to reflect the rapid redistribution of condensation the model underlay-node is placed in the centre of the underlay, giving for h_{1u} and h_{2u}

$$\begin{aligned} \frac{1}{h_{1u}} = r_{1u} &= \frac{1}{h_{bp1}} + \frac{r_{bp}}{2} \\ \frac{1}{h_{2u}} = r_{2u} &= \frac{1}{h_{bp2}} + \frac{r_{bp}}{2} \end{aligned} \quad (3)$$

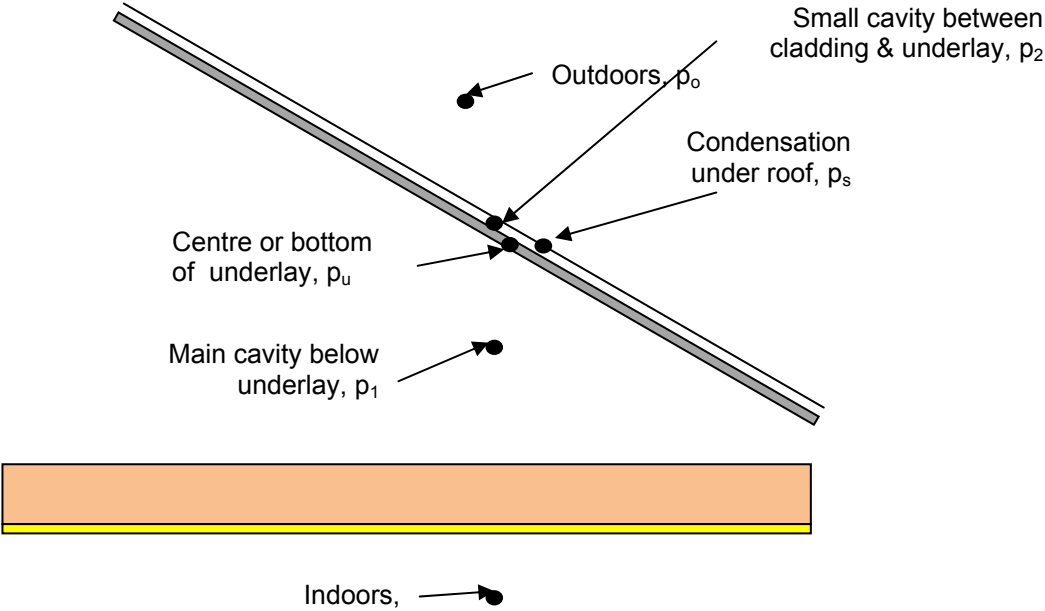
where h_{bp1} and h_{bp2} are surface mass transfer coefficients for bottom and top surfaces respectively, and r_{bp} is the vapour resistance of the underlay itself. However, for low hygroscopy synthetics, to model the condensation concentration on the under surface of the underlay the model underlay-node is placed on the bottom surface of the underlay, giving for h_{1u} and h_{2u}

$$\frac{1}{h_{1u}} = r_{1u} = \frac{1}{h_{bp1}} \tag{4}$$

$$\frac{1}{h_{2u}} = r_{2u} = \frac{1}{h_{bp2}} + r_{bp}$$



(a) Skillion roof



(b) Pitched roof

Figure 20:Roof types and model nodes

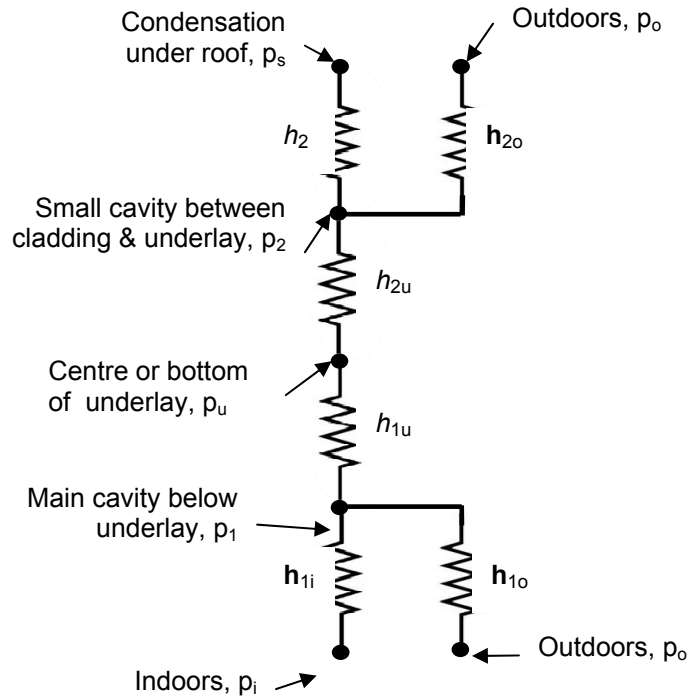


Figure 21: Model diagram

6.1.2 Model equations

Using the nomenclature shown in Figure 20 and Figure 21 mass balances are now calculated at each node giving

$$\begin{aligned}
 h_{1i}(p_i - p_1) + h_{1o}(p_{1o} - p_1) + h_{1u}(p_u - p_1) &= 0 \\
 h_{2s}(p_s - p_2) + h_{2o}(p_{2o} - p_2) + h_{2u}(p_u - p_2) &= 0 \\
 h_{1u}(p_1 - p_u) + h_{2u}(p_2 - p_u) &= \frac{\partial m_u}{\partial t} \quad (5)
 \end{aligned}$$

Note that it is being assumed that the vapour concentration in the cavities reaches equilibrium immediately, but the underlay can store moisture and so has a non-zero time-constant.

While the underlay has a moisture content less than the hygroscopic limit the sorption curve can be used to give a connection between the moisture content and the vapour pressure as follows

$$m_u = \left(\frac{\partial m}{\partial \varphi}\right) \varphi_u = \left(\frac{\partial m}{\partial \varphi}\right) \frac{p_u}{p_{sat}} = \lambda p_u \quad (6)$$

where $\left(\frac{\partial m}{\partial \varphi}\right)$ is the local slope of the sorption curve and where $\lambda = \left(\frac{\partial m}{\partial \varphi}\right) \frac{1}{p_{sat}}$.

Over a small range of temperature, moisture content and RH (in our case near 100%), λ in equation (6) can be taken as constant. Substituting (6) into equation (5) gives

$$\begin{aligned}
 h_{1i}(p_i - p_1) + \mathbf{h}_{1o}(p_{1o} - p_1) + h_{1u}(p_u - p_1) &= 0 \\
 h_{2s}(p_s - p_2) + \mathbf{h}_{2o}(p_{2o} - p_2) + h_{2u}(p_u - p_2) &= 0 \\
 h_{1u}(p_1 - p_u) + h_{2u}(p_2 - p_u) &= \lambda \frac{\partial p_u}{\partial t}
 \end{aligned} \tag{7}$$

Equations (7) have solutions

$$\begin{aligned}
 p_u &= \bar{p}_u + (p_u(0) - \bar{p}_u) \exp(-t/t_c) \\
 p_1 &= \bar{p}_1 + (p_1(0) - \bar{p}_1) \exp(-t/t_c) \\
 p_2 &= \bar{p}_2 + (p_2(0) - \bar{p}_2) \exp(-t/t_c)
 \end{aligned} \tag{8}$$

Here a bar over the top of the vapour pressures means the nominal final steady state value. This vapour pressure is called “nominal” because the actual vapour pressure may reach the saturated vapour pressure at the underlay’s temperature before it reaches the nominal vapour pressure.

The nominal final steady state vapour pressures are given by

$$\begin{aligned}
 \bar{p}_u &= \frac{H_i p_i + H_s p_s + (H_1 + H_2) p_o}{H_i + H_s + H_1 + H_2} \\
 \bar{p}_1 &= \frac{\mathbf{h}_{1i} p_i + \mathbf{h}_{1o} p_o + h_{1u} \bar{p}_u}{\mathbf{h}_{1i} + \mathbf{h}_{1o} + h_{1u}} \\
 \bar{p}_2 &= \frac{h_{2s} p_s + \mathbf{h}_{2o} p_o + h_{2u} \bar{p}_u}{h_{2s} + \mathbf{h}_{2o} + h_{2u}}
 \end{aligned} \tag{9}$$

where

$$H_i = \frac{\mathbf{h}_{1i} h_{1u}}{\mathbf{h}_{1i} + h_{1u} + \mathbf{h}_{1o}} \quad H_s = \frac{h_{2s} h_{2u}}{h_{2s} + h_{2u} + \mathbf{h}_{2o}} \quad H_1 = \frac{\mathbf{h}_{1o} h_{1u}}{\mathbf{h}_{1i} + h_{1u} + \mathbf{h}_{1o}} \quad H_2 = \frac{\mathbf{h}_{2o} h_{2u}}{h_{2s} + h_{2u} + \mathbf{h}_{2o}}$$

The sum of the H given in equation (9) is the total conductance seen from the point of view of the underlay and comes to

$$H_i + H_s + H_1 + H_2 = \{(\mathbf{h}_{1o} + \mathbf{h}_{1i}) \parallel h_{1u}\} + \{(\mathbf{h}_{2o} + h_{2s}) \parallel h_{2u}\} \tag{10}$$

where \parallel is the parallel operator defined as

$$a \parallel b = \frac{ab}{a + b}$$

It is useful to define a total resistance R as

$$R = 1/(H_i + H_s + H_1 + H_2)$$

allowing equation (10) to be rewritten as

$$R = (r_{1u} + \mathbf{r}_{1o} \parallel \mathbf{r}_{1i}) \parallel (r_{2u} + \mathbf{r}_{2o} \parallel r_{2s}) \quad (11)$$

Hence the steady state value of the underlay vapour pressure \bar{p}_u in equation (11) can be written as

$$\bar{p}_u = R(H_i p_i + H_s p_s + (H_1 + H_2) p_o)$$

The time-constant in equation (10) is given by

$$t_c = \lambda R \quad (12)$$

The initial underlay vapour pressure, $p_u(0)$ in equation (8) is taken as an independent variable. The initial values of the dependent variables $p_1(0)$ and $p_2(0)$ are given by replacing \bar{p}_u with $p_u(0)$ in equation (9).

6.2 Condensation mechanisms – no underlay

If there is no underlay then a different model applies as shown in Figure 22, which is the model of Figure 21 but without a roofing underlay.

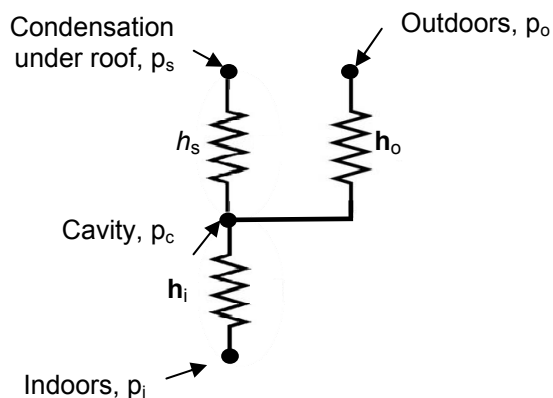


Figure 22: Model of a roof system without an underlay

This requires the vapour flow conduction to the outdoors of the two models to be related by

$$\mathbf{h}_o = \mathbf{h}_{1o} + \mathbf{h}_{2o}$$

The cavity vapour pressure for this model is

$$p_c = \frac{h_s p_s + \mathbf{h}_o p_o + \mathbf{h}_i p_i}{h_s + \mathbf{h}_o + \mathbf{h}_i}$$

If there is condensation appearing under the roof, the rate of condensation \dot{D} is given by

$$\dot{D} = h_s (p_c - p_s) \quad (13)$$

i.e.

$$\dot{D} = h_s \left(\frac{h_s p_s + \mathbf{h}_o p_o + \mathbf{h}_i p_i}{h_s + \mathbf{h}_o + \mathbf{h}_i} - p_s \right)$$

or

$$\dot{D} = h_s \| (\mathbf{h}_i + \mathbf{h}_o) (\bar{p}_c - p_s) \quad (14)$$

where

$$\bar{p}_c = \frac{\mathbf{h}_o p_o + \mathbf{h}_i p_i}{\mathbf{h}_o + \mathbf{h}_i}$$

6.3 Condensation mechanisms – high hygroscopy

A hygroscopic underlay controls condensation through three separate and successive mechanisms, viz.:

1. suppression of roof condensation through hygroscopic damping of local relative humidity
2. reduction of condensation rate through hygroscopic absorption
3. reduction of condensation rate through preventing high humidity lower cavity air direct contact with the metal roof

While mechanism 1 operates, both the underlay and the roof remain condensation free; while mechanism 2 operates, condensation appears under the roof but not on the underlay; and while mechanism 3 operates, condensation appears on both the underlay and the roof.

6.3.1 Suppression of roof condensation by hygroscopic damping of the local relative humidity

This is the first mechanism to operate as the metal roof cools through the night. Because the underlay is hygroscopic it controls the RH in the upper small cavity between the underlay and the roof. This keeps the dewpoint of the small cavity below the temperature of the roof, thus delaying the onset of condensation.

While there is no condensation, the roof system shown in Figure 21 must be modelled by excluding the flow path from the upper small cavity to the roof. In that case the vapour pressure of the small cavity is given by putting h_{2s} equal to zero in equation (9) giving

$$\bar{p}_2 = \frac{h_{2o}p_o + h_{2u}\bar{p}_u}{h_{2o} + h_{2u}} \quad (5)$$

As before $p_2(0)$ is given by replacing \bar{p}_u with $p_u(0)$ in the above equation (9). The time constant becomes

$$t'_c = \lambda R'$$

where R' from equation (11) is given by

$$R' = (r_{1u} + r_{1o} \| r_{1i}) \| (r_{2u} + r_{2o})$$

The period of time during which condensation is suppressed, t_σ , is found from the modified form of equation (8) with p_2 set to p_s and is given by

$$t_\sigma = t'_c \ln \left(\frac{\bar{p}_2 - p_2(0)}{\bar{p}_2 - p_s} \right)$$

If air change rates are low the time constant t'_c may be in the tens of hours. The potential for condensing will be at the most coldest part of the day, i.e. at night-time, and long before one time constant has passed it could be day again with the cessation of possible condensation. In this case condensing mechanisms 2 and 3 may never occur.

When condensation starts the underlay vapour pressure will be given by

$$p_u(t = t_\sigma) = \bar{p}_u + (p_u(0) - \bar{p}_u) \exp(-t_\sigma/t'_c) \quad (5)$$

where in this mode \bar{p}_u is given by putting h_{2s} equal to zero in equation (7).

6.3.2 Reduction of condensation rate through hygroscopic absorption

Once the small cavity air reaches the roof dewpoint, condensation begins under the metal roof. However, the underlay may still need to absorb hygroscopically considerable amounts of moisture before it is saturated. As the rate of condensation is directly related to the vapour pressure difference between the underlay and the roof, condensation rates will remain less than their maximum while the underlay is unsaturated.

While in this mode vapour pressures are given by equation (8) and the rate of accumulation of condensation under the roof, \dot{C} , is given by:

$$\dot{C} = h_{2s}(p_2 - p_s)$$

$$\text{i.e. } \dot{C} = h_{2s}(\bar{p}_2 - p_s + (p_2(0) - \bar{p}_2)\exp(-t/t_c)) \quad (17)$$

The time taken to saturate the underlay from equation (8) and (16) is

$$t_s = t_c \ln \left(\frac{\bar{p}_u - p_u(t = t_\sigma)}{\bar{p}_u - p_{us}} \right)$$

where p_{us} is the vapour pressure of the underlay when saturated.

The total amount condensed in this mode is given by integrating equation (17)

$$\begin{aligned} C &= \int_{t_\sigma}^{t_s} h_{2s}(\bar{p}_u - p_s + (p_2(0) - \bar{p}_2) \exp(-t/t_c)) dt \\ &= h_{2s} \{ (\bar{p}_u - p_s)(t_s - t_\sigma) + t_c(\bar{p}_2 - p_2(0))(\exp(-t_s/t_c) - \exp(-t_\sigma/t_c)) \} \end{aligned}$$

6.3.3 Prevention of contact of lower cavity air with the roof

Here the vapour resistance of the underlay intervenes between the large lower cavity and the roof, reducing the flow of moisture available for condensing.

The condensation rate under the roof while in this mode is

$$\dot{C} = h_{2s}(\bar{p}_2 - p_s) \quad (18)$$

where, while in this mode small upper cavity vapour pressure takes the value \bar{p}_2 given by

$$\bar{p}_2 = \frac{h_{2s}p_s + h_{2o}p_o + h_{2u}p_{us}}{h_{2s} + h_{2o} + h_{2u}}$$

Equation (18) can also be written as

$$\dot{C} = h_{2s} \parallel (h_{2o} + h_{2u})(\bar{p}_2 - p_s)$$

where \bar{p}_2 is defined by equation (15).

In this mode condensation is forming both under the roof but also under the underlay. Moisture is condensing under the underlay from vapour flow from the lower large cavity and is being lost to evaporation to the upper cavity with a net condensation rate given by

$$\dot{E} = h_{1u}(\bar{p}_1 - p_{us}) - h_{2u}(p_{us} - \bar{p}_2) \quad (19)$$

where, while in this mode, p_1 takes the value \bar{p}_1 given by

$$\bar{p}_1 = \frac{h_{1i}p_i + h_{1o}p_o + h_{1u}p_{us}}{h_{1i} + h_{1o} + h_{1u}}$$

Equation (19) can also be written as

$$\dot{E} = h_{1u} \parallel (h_{1i} + h_{1o})(\bar{p}_1 - p_{us}) - h_{2u} \parallel (h_{2s} + h_{2o})(p_{us} - \bar{p}_2)$$

where

$$\tilde{p}_1 = \frac{h_{1i}p_i + h_{1o}p_o}{h_{1i} + h_{1o}}$$

and

$$\tilde{p}_2 = \frac{h_{2s}p_s + h_{2o}p_o}{h_{2s} + h_{2o}}$$

6.4 Condensation mechanisms – low hygroscopy

With low hygroscopy underlays mechanisms 1 and 2 above do not apply and only the third mechanism operates, i.e. the underlay protects the roof by reducing the amount of condensation that appears there at the expense of experiencing condensation itself.

The rate of condensation onto the roof will be given by equation (18), while if there was no underlay the rate onto the roof would be given as before by equation (18). When doing this modelling it must be remembered to use the low hygroscopy expressions for h_{1u} and h_{2u} given by equation (4), not those for hygroscopic underlays given by equation (3).

Figure 23 shows the reduction in roof condensation rate as a function of vapour resistance for a low hygroscopy underlay. The particular roof considered is the one described in the examples below, parameterised by data in Table 7, Table 8 and Table 9.

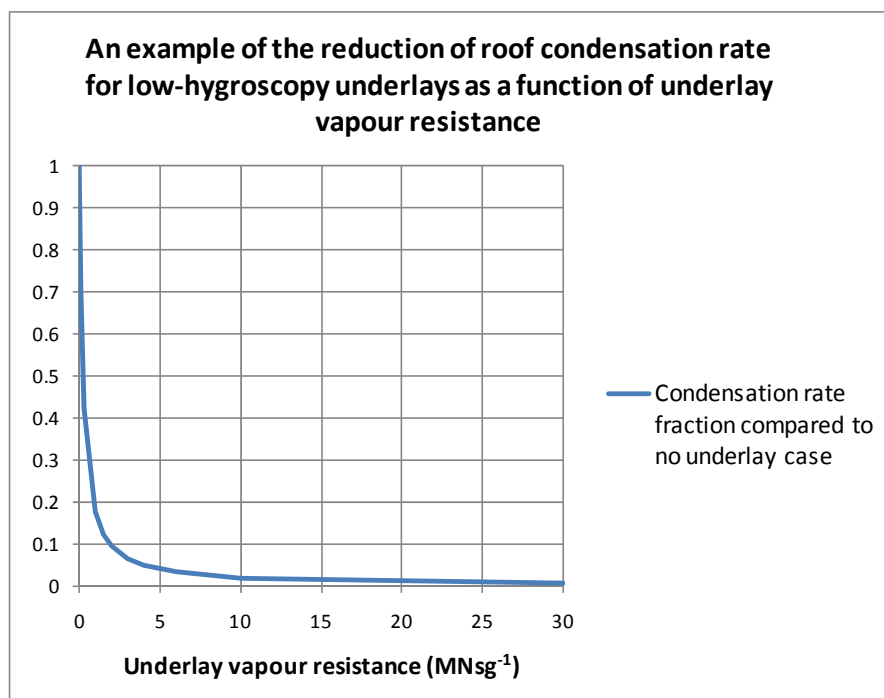


Figure 23 An example of the reduction of roof condensation rate for low hygroscopy underlays as a function of underlay vapour resistance

6.5 Examples

6.5.1 Skillion roof with a Kraft underlay

A Kraft paper underlay is considered with the following parameters:

- R-values given in Table 7.
- Roof parameters given in Table 8.

- Psychrometric parameters are given in Table 9
- Underlay parameters are given in Table 10

Figure 24 and Figure 25 show the vapour pressures, condensation and condensation rates as calculated for this model. Figure 26 shows how the roof condensation and underlay condensation compare to the no underlay case.

6.5.2 Non-hygroscopic underlay

This non-hygroscopic underlay has the parameters given in Table 6. Since the underlay is non-hygroscopic there are no parameters for the saturation level and the hygroscopic parameter λ . R-values, roof parameters and psychrometric parameters are the same as the previous example.

Table 6: Underlay (non-hygroscopic) parameters

Area density	0.14 kg m ⁻²
Vapour resistance (r_{bp})	24.6E+09 Nskg ⁻¹

Figure 27 and Figure 28 show the vapour pressures, condensation and condensation rates as calculated for this model. Figure 29 shows how the roof condensation and underlay condensation compare to the no underlay case.

It can be seen in Figure 29 that using a low-hygroscopy moderately high vapour resistance underlay, almost all the condensation is appearing under the underlay and the amount accumulating is not much less than that which appears under the roof when there is no underlay. The underlay in effect has shifted the condensation plane from under the roof to under the underlay, reducing the corrosion threat to the roof, and because of the holding power of the underlay, reducing the likelihood of drip deeper into the roof structure.

Table 7: Thermal properties of the example roof

	R-value (m ² °C/W)
Indoor Surface	0.1
Gib	0.03
50mm batts	1.25
Cavity1	0.15
Underlay	0
Cavity2	0.1
Surface	0.05

Table 8: Example roof parameters

h_{1i}	4.424E-10 kg N ⁻¹ s ⁻¹
h_{1o}	1.091E-11 kg N ⁻¹ s ⁻¹
h_{2s}	1.000E-08 kg N ⁻¹ s ⁻¹
h_{2o}	1.097E-12 kg N ⁻¹ s ⁻¹
F_{1i}	1ach
F_{1o}	0.1ach
F_{2o}	0.1ach
V_1	0.05 m ³ (per metre of length)
V_2	0.005 m ³ (per metre of length)
R, calculated from equation (11)	2.599E+09 kg N ⁻¹ s ⁻¹

Table 9: Psychrometric parameters

Indoor temperature T_i	20 °C
Outdoor temperature T_o	0 °C
Under roof temperature T_s	1 °C
Indoor relative humidity RH_i	50%
Outdoor relative humidity RH_o	90%
Indoor vapour pressure P_i	1168 Pa
Outdoor vapour pressure P_o	549 Pa

Table 10: Underlay (hygroscopic) parameters

Area density	0.37 kg m ⁻²
Saturation	14%
Vapour resistance (r_{bp})	0.60E+09 Nskg ⁻¹
λ , calculated from equation (6)	7.001E-05 kgN ⁻¹
t_c , calculated from equation (12)	50.53 h

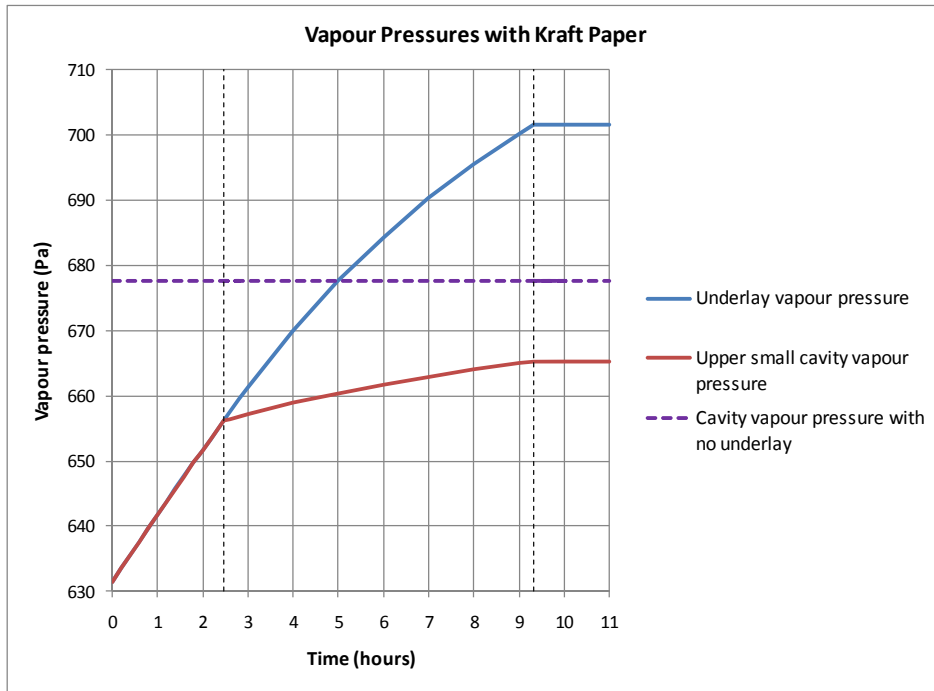


Figure 24: Vapour pressures with Kraft paper. The vertical dashed lines mark the boundaries between the three regimes (see text)

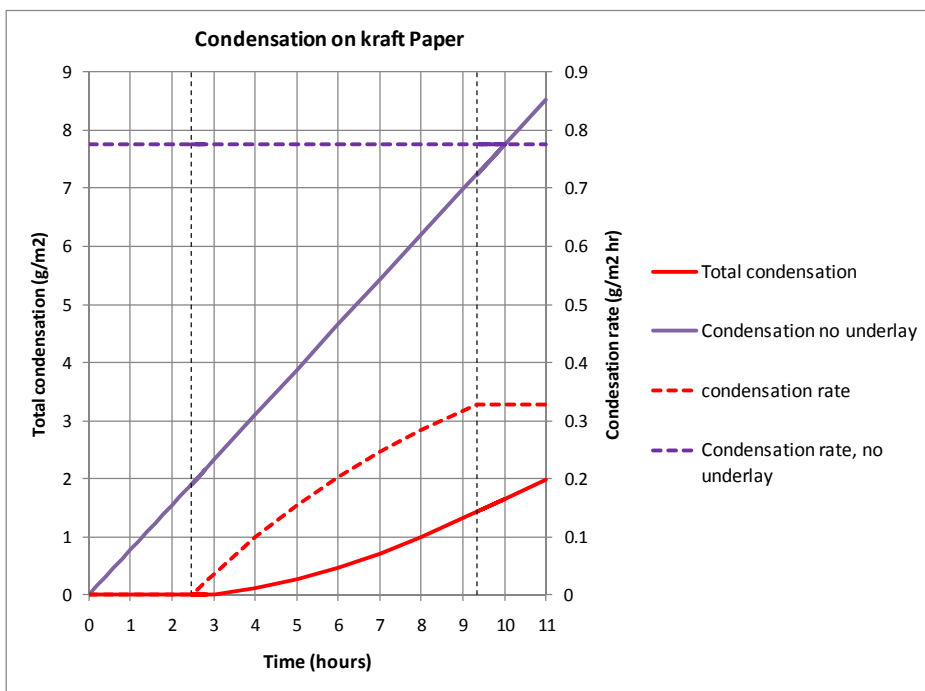


Figure 25: Condensation and condensation rates with kraft paper. The vertical dashed lines mark the boundaries between the three regimes, see text.

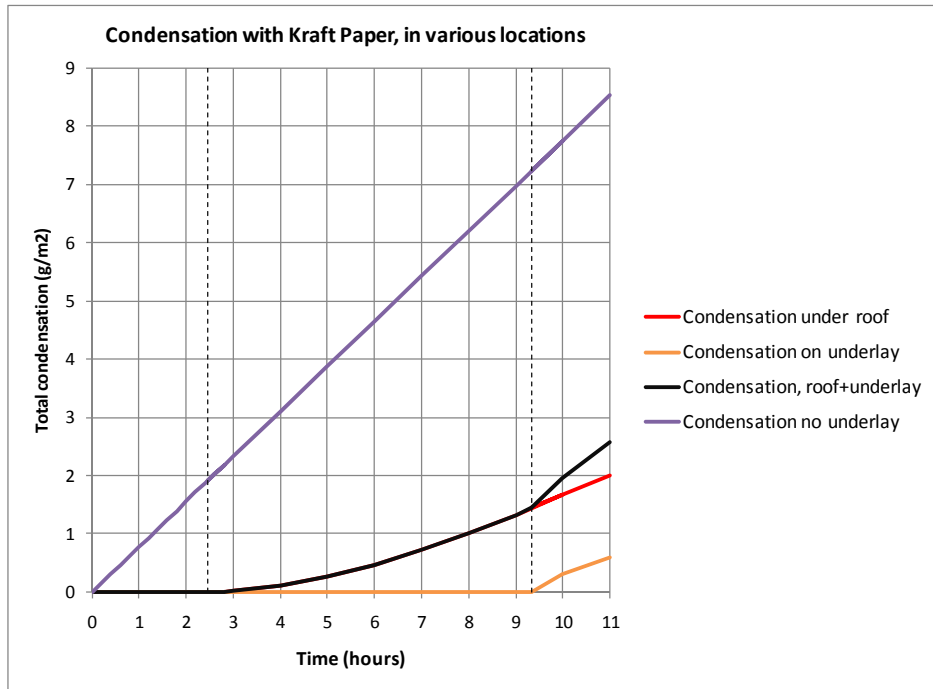


Figure 26: Condensation with Kraft paper on the underlay, the roof, and in the case of no underlay. The vertical dashed lines mark the boundaries between the three regimes (see text)

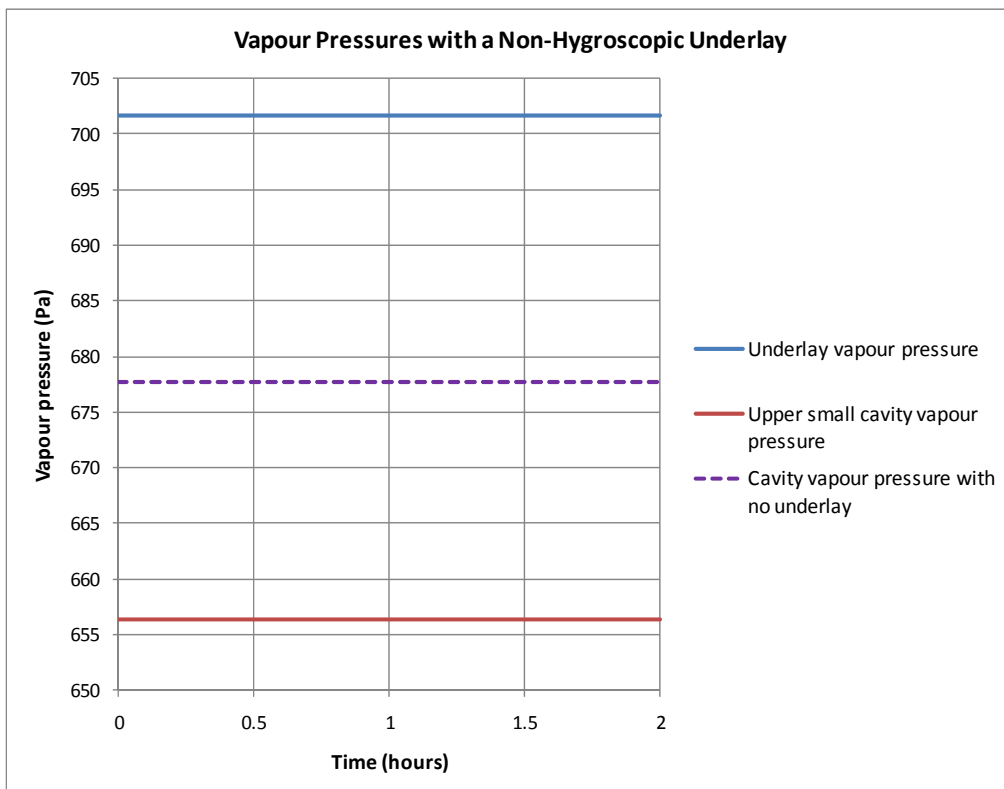


Figure 27: Vapour pressures with non-hygroscopic underlay

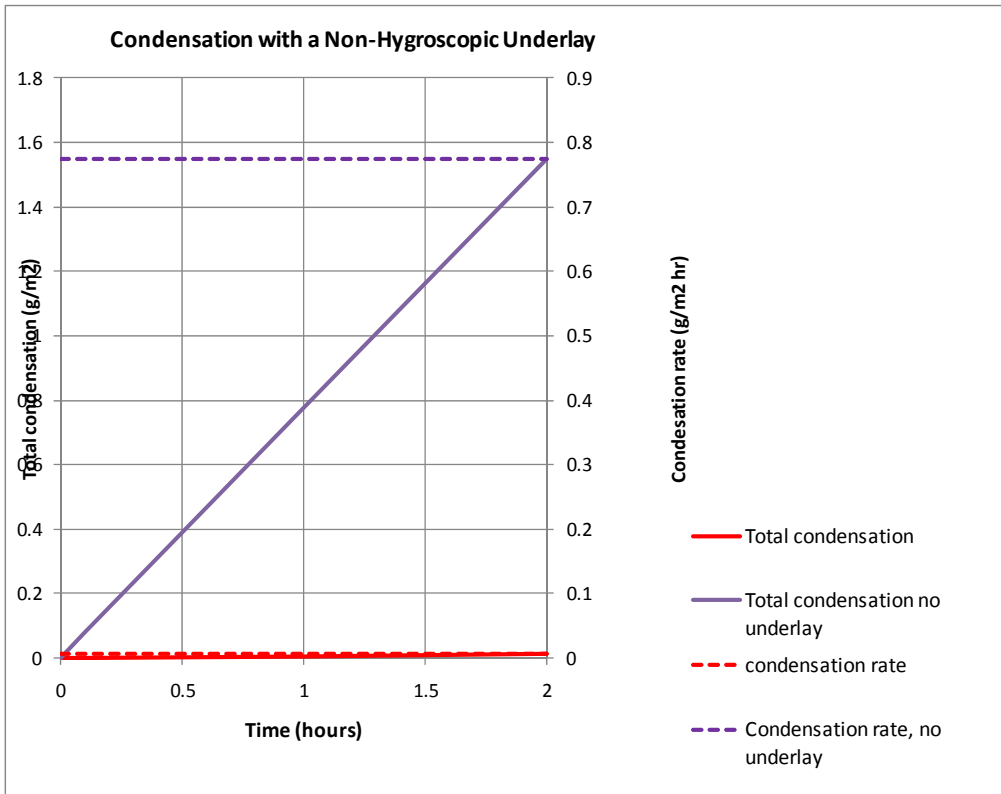


Figure 28: Condensation and condensation rates with non-hygroscopic underlay

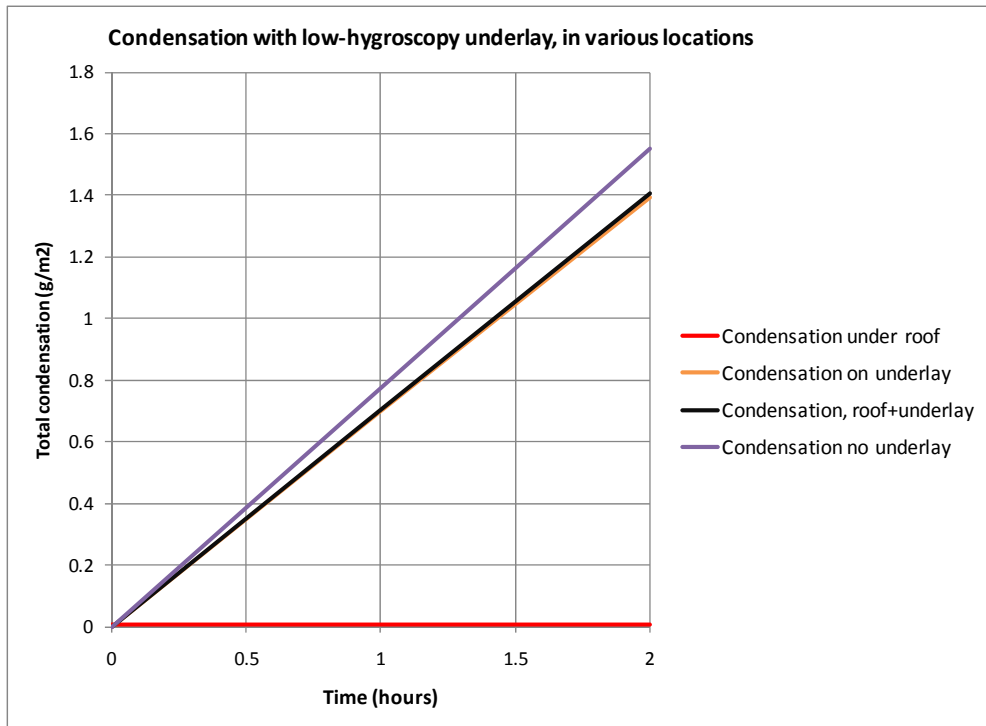


Figure 29: Condensation with low hygroscopy underlay, on the underlay, the roof, and in the case of no underlay

7. STUDY OF ROOF UNDERLAY ACTING AS A CONDENSATION PLANE

7.1 Introduction

Roof underlays which exhibit a high liquid penetration resistance are adequate to prevent condensation from passing through to the timber framing or the insulation if condensation collects in the region above the underlay.

But modelling has shown that, especially under conditions of night sky radiation, condensation could also form on the underside of the underlay while moisture is migrating from the inside towards the outside of the structure. When this happens condensation forms, in a certain sense, on the “wrong” side of the underlay and all the considerations described in the previous chapters do not hold anymore. In this situation the roof underlay has to be able to prevent the condensation from dripping by some mechanism other than resisting liquid penetration.

A possible mechanism is that water droplets are held in place simply by surface tension. Condensation always starts as a very thin film which evolves into small water droplets which then coalesce into bigger water droplets. The surface tension determines the contact angle of the water droplets to the surface, which in turn influences the shape of the water droplets and consequently the maximum amount of condensation the underlay can hold in place.

Paper-based underlays have a well pronounced sorption curve and can store part of the moisture within the body of the membrane in the form of bound water. This mechanism, as seen in the analytical model, has the effect of delaying the formation of water droplets on the underside of the underlay. Synthetic underlays, on the contrary, have negligible hygroscopic properties and mainly store moisture at the surface of the underside of the membrane. Moreover the surface of some synthetic underlays is covered in small indentations where water can collect in the form of small beads.

In order to study the behaviour of different underlays under the situation of condensation forming on the underside of the membrane, a laboratory experiment has been set-up in a climate chamber. Details and results are expounded in the following paragraphs.

7.2 Climate chamber condensation experiment

To create condensation on the underside of a specimen of underlay, it is necessary to create a situation in which the underside of the underlay has a temperature below the dew point of the air just underneath it. In order to achieve this situation, the experimental set-up depicted in Figure 30 to Figure 33 has been used. This set-up tries to mimic the characteristic of a pitch roof with metallic cladding and with roof space.

A square piece of underlay is clamped to a sloping metallic frame to simulate a pitch roof (Figure 31). The three sides and the floor of the metallic frame are sealed with plastic sheets to recreate a confined space similar to a roof space. A tray of water with a heater is installed in the confined space (Figure 30). Heating the water to a constant temperature raises and stabilises the temperature and the RH in the confined volume. A flat metallic plate is laid on top of polystyrene edge which sits on the perimeter of the underlay to simulate a metallic cladding (Figure 33). The polystyrene edge creates a cavity between the upper side of the underlay and the metallic plate and insulates it from the outside (Figure 32).

All this set-up is placed in a climate chamber. The temperature of the water in the tray inside the confined space is set at 30 °C and it is actively controlled so as to stay stable. The temperature of the climate chamber is set to 10 °C. As the upper side of the metallic plate is exposed to the cool air in the climate chamber, it cools and drives the

cooling of the air in the cavity and of the underlay. This recreates the situation of a roof exposed to cold air on the outside, but with a warmer and humid roof space. The temperatures of the water and of the climate chamber have been selected for practical reasons in order not to overcome the cooling capability of the climate chamber. With these temperature settings, the temperature of the underside of the underlay specimen is below the dewpoint and condensation forms quite quickly.

Temperatures and RHs are continuously monitored at several locations in order to make sure that a steady state situation is reached and that it can be repeated while testing the behaviour of different underlays. The main measurements are gravimetric measurements of the amount of condensation accumulated on the underside of the underlay and on the underside of the metallic plate. In order to facilitate and accelerate the gravimetric measurements, so as not to perturb too much the steady state conditions in the climate chamber, the specimen of underlay was fixed with magnetic strips to an edge made of thin plastic which is permanently clamped to the metallic frame. Every hour the condensation on the metallic plate is wiped with a paper towel and weighted, and the underlay specimen is weighted as a whole making sure that no condensation is accidentally lost in the process.

These gravimetric measurements allow studying of the formation and the evolution of the condensation process on the underside of the underlay, but also the effect the underlay has on formation of condensation on the cladding.

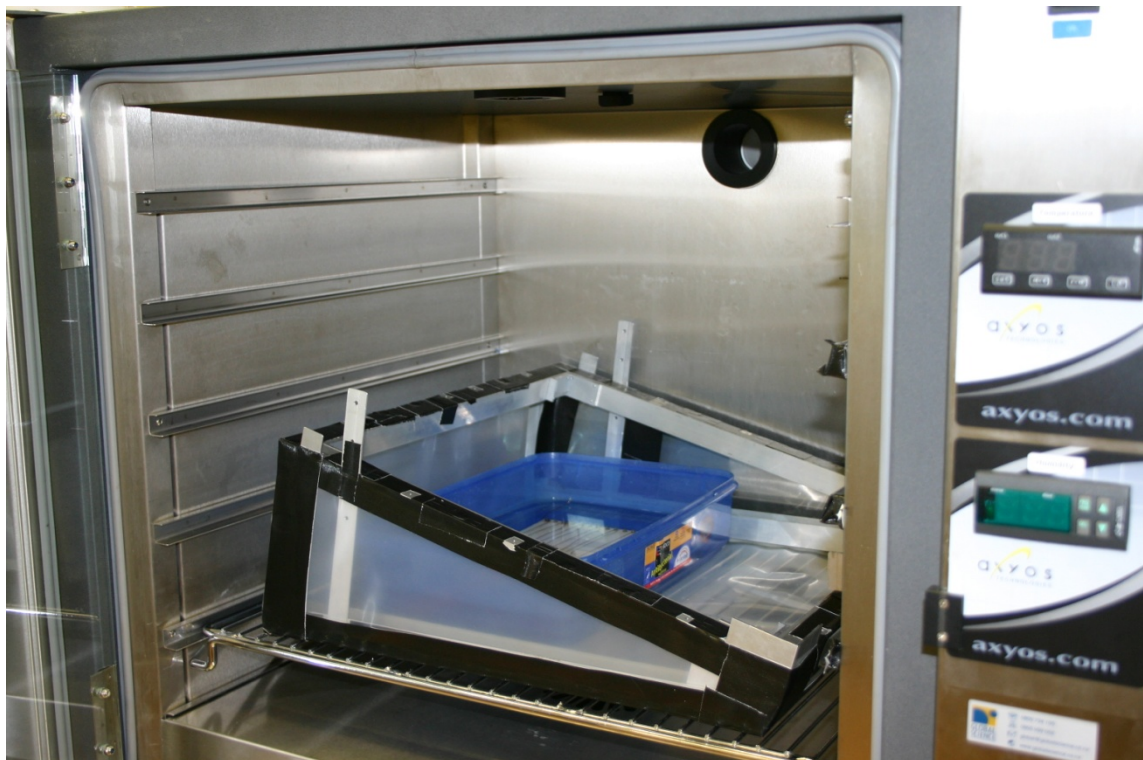


Figure 30: Metal frame used to support the underlay specimen. The sides of the metal frame are sealed to create a confined space. A tray of water with a flat heater provides the source of moisture

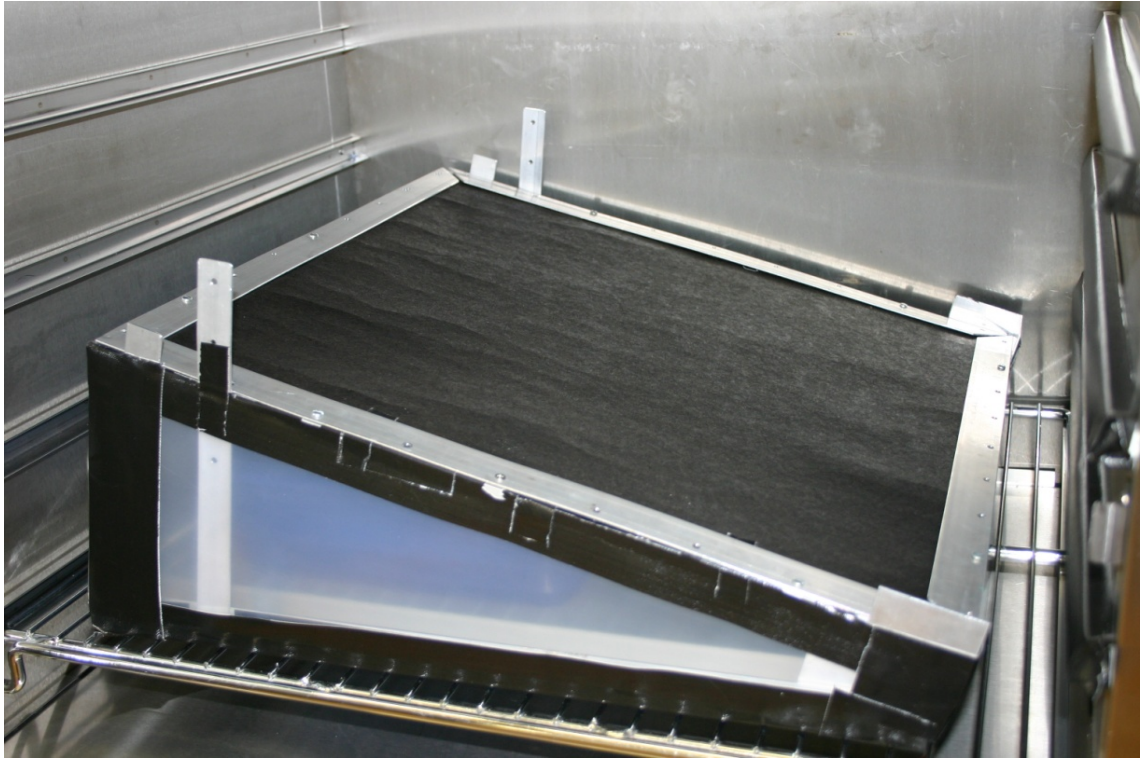


Figure 31: The underlay specimen clamped to the metal frame. This set-up aims to reproduce the equivalent of a very moist roof space



Figure 32: Polystyrene enclosure supporting a metal plate and creating a cavity above the underlay specimen



Figure 33: Metal plate simulating a metal cladding installed above the underlay specimen

7.3 Experimental results: condensation on the underside of the metal plate

Several underlays with different characteristics have been tested under the same driving conditions and with the set-up described above. The same naming convention for roof underlays adopted in Chapter 2 has been used here.

These underlays have been chosen to give a sample of wraps with contrasting characteristics. Wrap F is the traditional Kraft paper, Wrap C is synthetic and has low water vapour resistance and high absorbency, Wrap D is synthetic and has low vapour resistance and low absorbency, and Wrap J is synthetic and has high water vapour resistance and low absorbency. The case of a synthetic underlay with high water vapour resistance and high absorbency was not found among all the roof underlays available to us.

The summary of several series of experimental runs, under the same conditions is presented in Figure 34 and Figure 35. The graph of the condensation accumulation on the metal plate shows that Wrap C, Wrap D and Wrap F behave similarly contrasting the behaviour of Wrap J. When Wrap C, Wrap D and Wrap F are tested, condensation appears since the initial phases of the experiment on the metal plate. Rates of accumulation are nevertheless different.

According to the analytical model presented in Chapter 6 the condensation rate on the underside of the metal surface depends on the water vapour resistance of the underlay. Wrap C has a water vapour resistance of 0.30 MN s/g, Wrap D of 0.40 MN s/g and Wrap F of 0.60 MN s/g. The higher the water vapour resistance the less the condensation rate should be. The experimental results agree with this observation. Wrap F is a paper-based underlay with a very well-pronounced sorption curve. The analytical model predicts that in the first phases of the condensation experiment no condensation should appear on the underside of the metal. In Figure 34 it can be seen

that the condensation rate is null or nearly null during the first two hours or so of the experiment. This confirms the accuracy of the predictions of the analytical model.

When Wrap J is tested, very little condensation is observed on the underside of the metal. The water vapour resistance of the underlay is 110 MN s/g. The analytical model correctly forecasts that very little condensation should be observed. There is here an argument for having roof underlays with a water vapour resistance a bit higher than 1 MN s/g in order to benefit from the fact that condensation on the metal could be noticeably reduced as seen from the analytical model.

7.4 Experimental results: condensation on the underside of the underlay

The graph of the condensation accumulation on the underside of the underlay indicates that Wrap C, Wrap D and Wrap J behave in a similar way while Wrap F differentiates itself from the others.

Wrap F is the traditional Kraft paper and, differently from synthetic underlays, it has a well pronounced hygroscopic sorption curve as can be seen in Figure 36 where Wrap F and Wrap C (representative of synthetic underlays) are compared.

Synthetic underlays have a very limited ability to store moisture hygroscopically and the only way they can “absorb” moisture is when moisture is in liquid form (condensation). Moisture is then held at the surface of the membrane by surface tension as unbound water. The sharp rise in moisture content of Wrap C seen at 100% RH is the signature of this phenomenon.

Kraft paper can store a significant amount of moisture in its structure according to its sorption curve and depending on RH. In Figure 35 it is seen that in the first hour of the experiment, Kraft paper is able to absorb a bit more than 10 g/m² of moisture while the synthetic underlays only hold around 1-2 g/m² of moisture. But after this first hour, the mass increase of all underlays is similar, with a rate of around 5 g/(m² h).

We can interpret this result in the following way. After an initial transient of around one hour, condensation accumulates on the underside of all underlays tested at a rate of 5 g/(m² h). Due to the characteristics of synthetic underlay, condensation remains a surface phenomenon for Wrap C, Wrap D and Wrap J. In the case of Kraft paper, moisture is hygroscopically adsorbed during the first hour, but then condensation mainly forms on the underside of the membrane with only limited further hygroscopic adsorption.

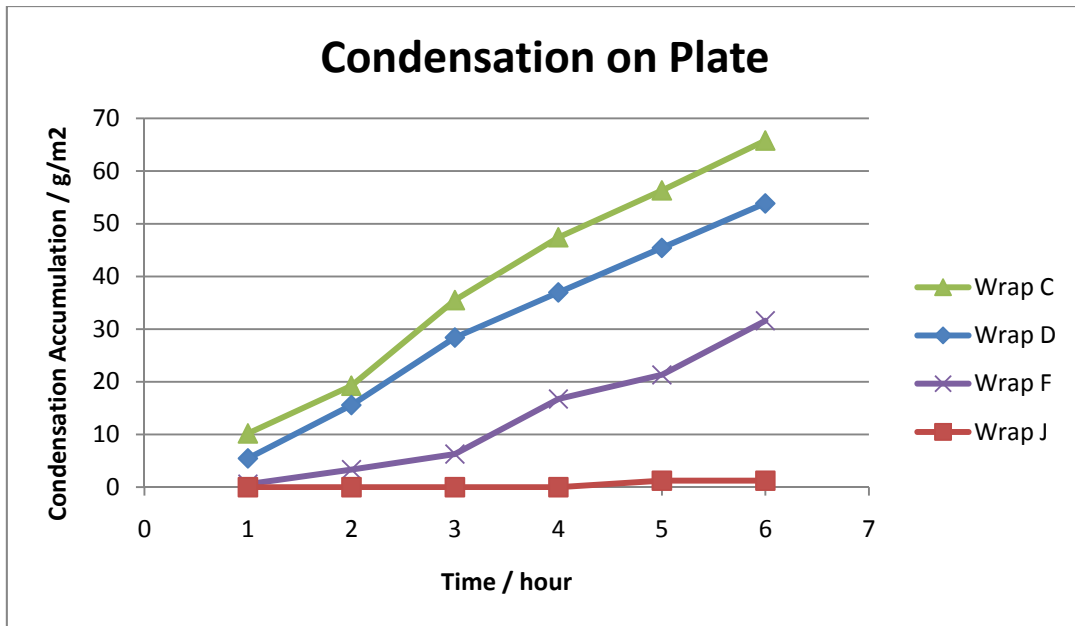


Figure 34: Condensation accumulation on the underside of the metal plate during the climate chamber condensation experiment.

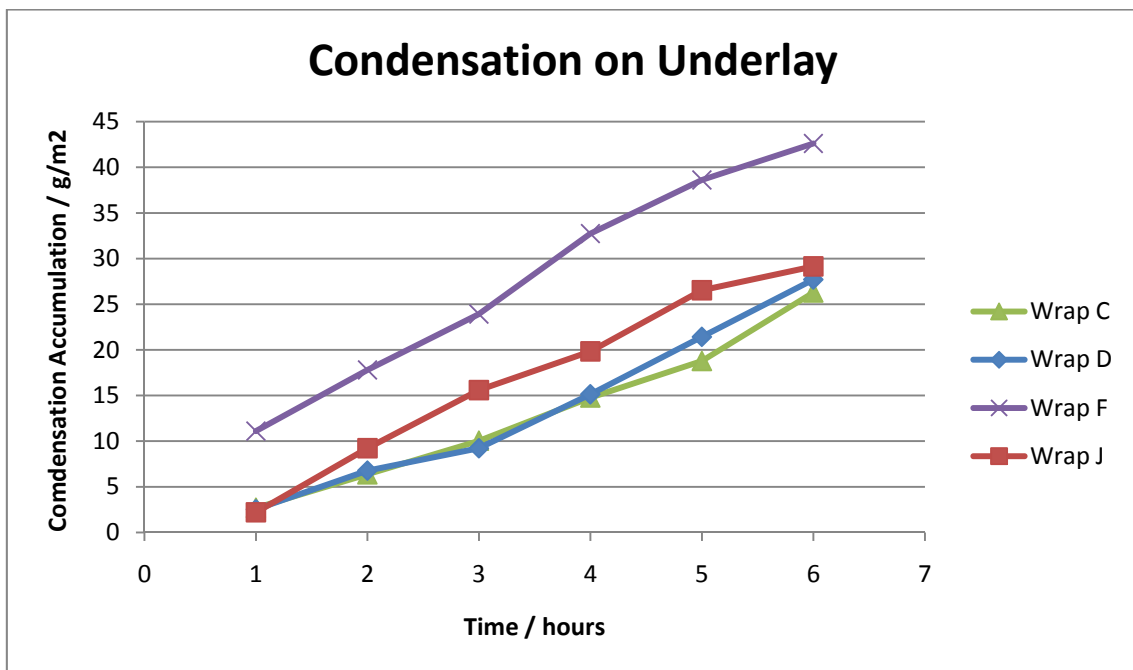


Figure 35: Condensation accumulation on the underside of the underlay for several membranes during the climate chamber condensation experiment.

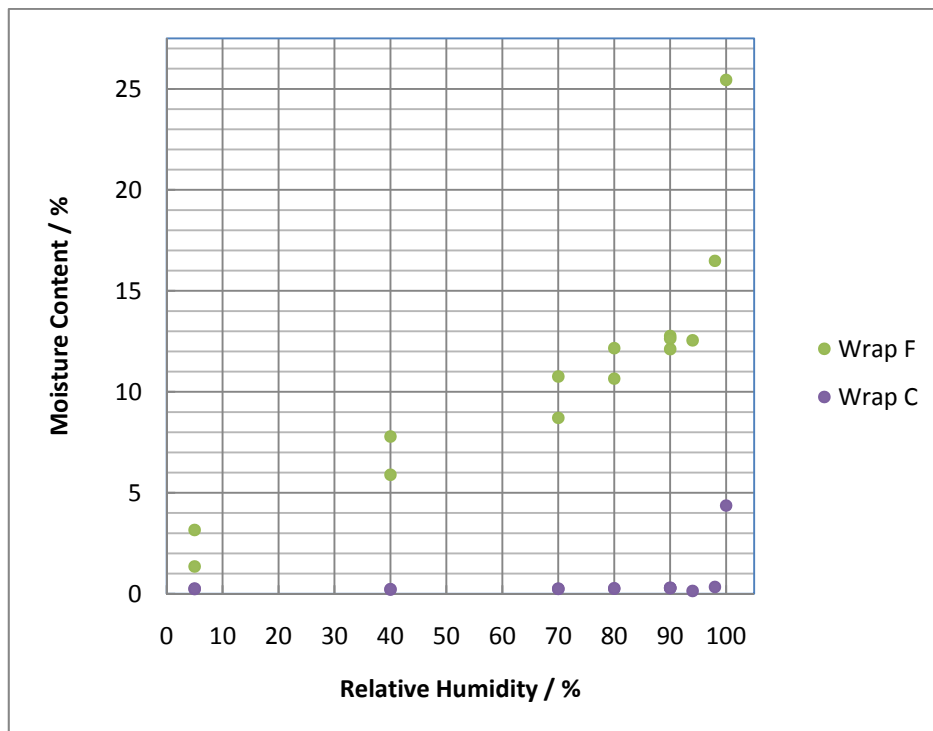


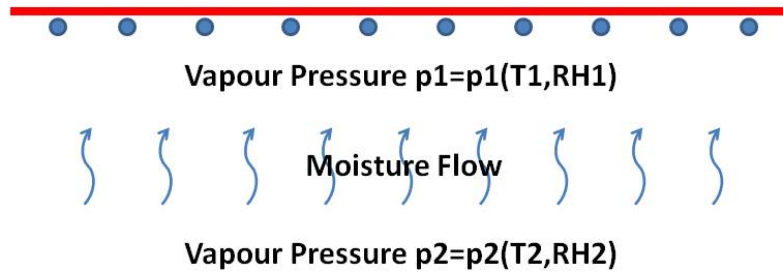
Figure 36: Comparison between the hygroscopic sorption curve of a synthetic wrap (Wrap C) and a paper-based wrap (Wrap F)

The main result of the analysis of the experimental results presented in Figure 35 is that condensation on the underside of roof underlays, paper-based or synthetic, is a surface phenomenon.

In further analysis, we can estimate the surface mass transfer coefficient. In a steady state situation, there is a moisture flow, driven by differential in vapour pressure, from the moist air underneath the underside of the underlay and the underside of the underlay. The surface temperature of the underlay is below the dew point of air and the process of condensation can take place. The condensation rate is directly proportional to the vapour pressure differential and the proportionality constant is the mass transfer coefficient. The situation is depicted in Figure 37.

The condensation rate has been estimated at $5 \text{ g}/(\text{m}^2 \text{ h})$. Figure 38 and Figure 39 display the steady state hygrothermal conditions in proximity of the underside of the underlay and of the air underneath the underlay during the climate chamber condensation experiment. The temperature of the underlay is around $22.5 \text{ }^\circ\text{C}$ and the temperature of the air around $23.6 \text{ }^\circ\text{C}$. The RH sensor, which is at just 1-2 mm from the surface of the underlay indicates 96%RH. This value is probably more representative of the condition of the boundary layer of air influencing the condensation than the value 93% recorded by a more bulkier sensor at about half a centimetre from the surface of the underlay. Using the values $T_1=22.5\text{C}$, $\text{RH}_1=100\%$ (because there is a condensing situation at the very surface of the underlay), $T_2=23.6\text{C}$, $\text{RH}_2=96\%$ and the condensation rate $5 \text{ g}/(\text{m}^2 \text{ h})$, the surface mass transfer coefficient can be estimated at around $2 \cdot 10^{-8} \text{ kg}/(\text{m}^2 \text{ s Pa})$.

UNDERLAY



$$\text{Condensation Rate} = h (p_2 - p_1)$$

Figure 37: Schematic of the driving forces creating an accumulation of condensation on the underside of the underlay. The vapour pressures depend on the temperature T and on the RH . The surface mass transfer coefficient is represented by the constant h . The condensation rate is then proportional to the surface mass transfer coefficient and to the differential in vapour pressures

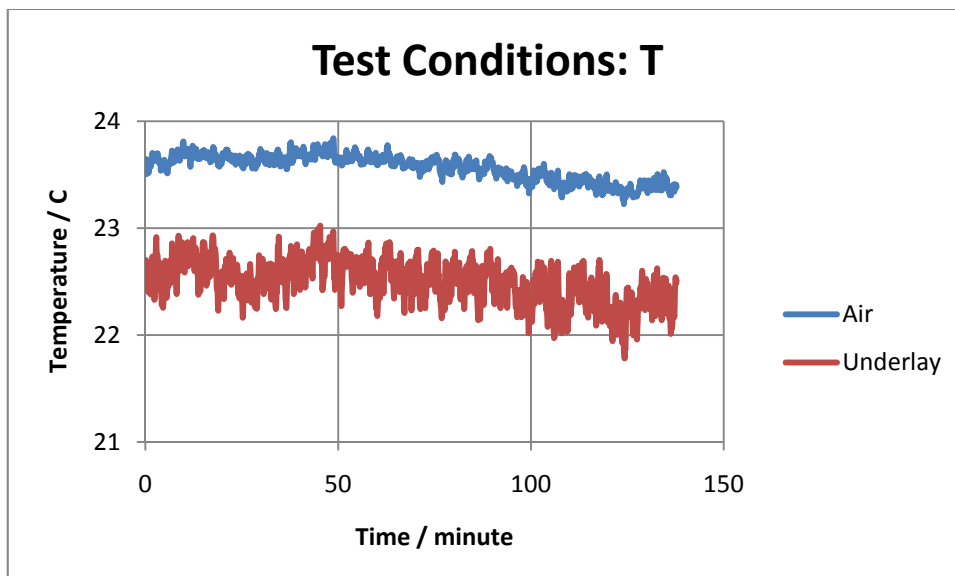


Figure 38: Thermal conditions near the underside of underlay specimens during the climate chamber condensation experiment

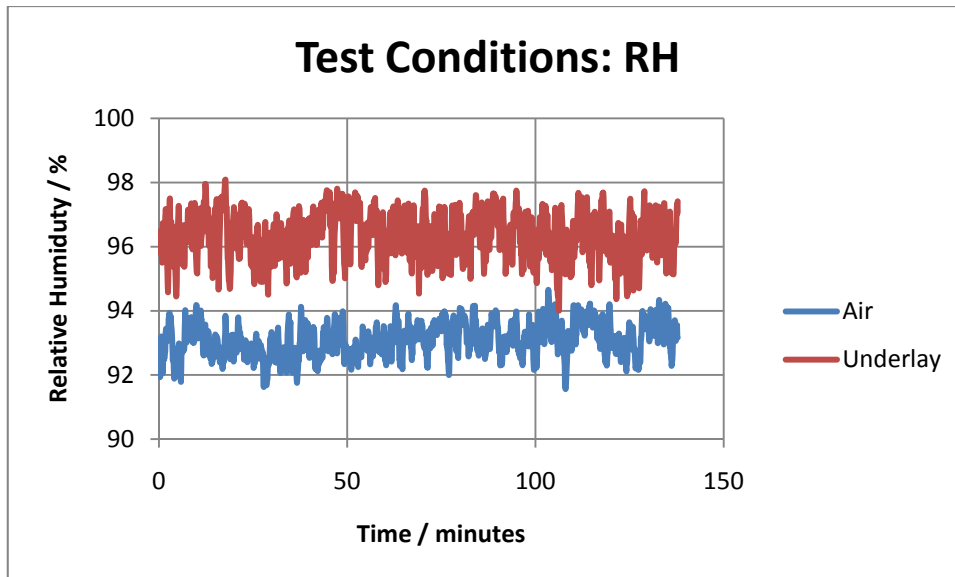


Figure 39: Hygroscopic conditions near the underside of the underlay specimen in the climate chamber condensation experiment

7.5 Measurement of mass transfer coefficients

To compare the different underlays and indirectly confirm that condensation on the underside of the underlay mainly takes place as a surface phenomenon, the surface mass transfer coefficient of a range of membranes was measured.

The surface mass transfer coefficient is the same for condensation and for evaporation. As it is easier, for practical reasons, to study evaporation than condensation, the following experiment was set up. The idea of the measurement is to follow the change in weight of an underlay which is completely soaked in water while water is evaporating away from it. The surface mass transfer coefficient can then be calculated starting from this data.

The measurements were carried out in a climate-controlled room with pretty constant temperature and RH. This ensures that the drivers of the evaporation process stay roughly constant.

A square sample 200 x200 mm was completely immersed in a tray of distilled water and let soak for 24 hours. After that period, the sample was taken out of the water and put on a digital scale. The weight of the sample was then logged at regular interval (five seconds) in order to follow the evolution of the weight during the evaporation process. An example of the data obtained is presented in Fig. and in Fig.

Water can be present as unbound water on the surface of the underlay or as bound water in the body of the underlay. The evaporation of unbound water under constant driving forces should produce a linear decrease of the weight of the underlay. The simultaneous evaporation of unbound water and of bound water gives rise to a more complex behaviour.

The result of these measurements is shown in Table 11.

Table 11: Surface mass transfer coefficient of a range of building wraps

Wrap	Surface Mass Transfer Coefficient (kg/m ² s Pa)
Wrap C	$2.6 \cdot 10^{-8}$
Wrap D	$2.0 \cdot 10^{-8}$
Wrap E	$2.4 \cdot 10^{-8}$
Wrap F	$2.5 \cdot 10^{-8}$
Wrap J	$2.5 \cdot 10^{-8}$

The surface mass transfer coefficients of the range of underlays tested are quite similar. This indirectly confirms the experimental results of Figure 35. Putting aside Wrap F, which is paper-based, synthetic underlays behave in a very similar way. Condensation on the underside of the underlay is in this case a purely surface phenomenon and it is regulated by the value of the surface mass transfer coefficient.

7.6 Conclusions

Liquid penetration resistance has been identified as the most important property for dealing with liquid collecting on the upper side of the underlay. If condensation forms on the underside of the underlay, the main mechanism which allows retaining moisture is surface tension. Several synthetic underlays with high and low water vapour resistance and with high and low absorbency (in the sense of AS/NZS 4201.6) have been tested and they all behaved in a similar manner in regard to the amount of condensation accumulating on the underside of the membrane (Figure 35). This observation points to the fact that absorbency and water vapour resistance have very little influence on the formation of condensation on the underside of the underlay. This is understandable looking at the fact that condensation has been shown to be a surface phenomenon.

As seen in the analytical model, if the underlay has a pronounced hygroscopic behaviour (as is the case for paper-based membranes, e.g. Wrap F), the onset of surface condensation is noticeably delayed. On the contrary, in the case of synthetic underlays which are only marginally hygroscopic, condensation appears much sooner.

The value of water vapour resistance has an influence on the amount of condensation accumulating on the metal cladding. The analytical model suggests that increasing the value of water vapour resistance a bit above 1-2 MN s/g could offer a significant reduction of condensation under the metal cladding.

8. PROPOSAL FOR A NEW “SURFACE WATER NO-DRIP TEST”

8.1 Introduction

It has been repeatedly shown that absorbency as it is measured according to the Standard AS/NZS 4201.6 bears little similarity with what happens in the field. The fact that an underlay has a high absorbency has not shown up as giving a clear benefit or advantage in any of the cases studied.

Rather, two important characteristics of roof underlays need to be identified: the resistance to water penetration from the upper side; and the ability to hold surface moisture on the underside. A good test is already available for the liquid water penetration. A test for the second property does not exist.

Hereby it is proposed a new test that could be named “Surface Water No-Drip Test”. Its aim is to quantify how much surface moisture can be held by surface tension on the underside of the underlay before drip commences.

8.2 Description of the experimental set-up

The aim of the test is to accumulate condensation on the underside of a sample of underlay and detect when drip starts. A possible experimental set-up is shown in Figure 40. A tray of water with a heater (similar to the one used for the climate chamber condensation experiment shown in Figure 30) is used as a controllable moisture source. A square 200 x 200 mm sample of underlay is suspended just above the surface of the water on the hook of a digital scale.

The water in the water tray is first heated to 60 °C and kept to this temperature for the whole test by means of a controllable power supply. This temperature has been found adequate to achieve a relatively fast condensation rate on the underside of the underlay sample without being too hot to damage the specimen. Only after the water in the tray has reached equilibrium is the specimen hung to the scale. The specimen is supported by a Plexiglas frame connected by four wires to the hook under the scale, as shown in detail in Figure 41. The underlay specimen lies quite close to the surface of the water, just 1-2 cm above it, at the same level as the top of the tray. As seen in Figure 41, part of the top of the water tray is covered by a plastic sheet so to create an opening which is just a bit bigger than the dimension of the underlay specimen. This guarded area has the function of helping create dissimilar conditions for the underside and the upper side of the underlay. The underside of the specimen is exposed to the high RH and temperature created by the heating of the water. The upper side is more influenced by the cooler and drier air of the room where the experiment is located. The cooling of the upper side of the sample keeps the underside of the specimen below the dew point of the underlying warm and moist air and sustains the condensation of moisture on the underside of the underlay.

The weight of the specimen is then logged every five seconds using a LabVIEW software during the entire duration of the test (Figure 42). When the test can be considered finished is explored in the next section.

8.3 Some theoretical considerations

It is expected that initially the weight of the underlay specimen will rise at a constant rate due to the constant flow of moisture generated by the heated water in the tray. But at a certain point the amount of condensation will reach a level that will trigger dripping of water. In Figure 43 this situation is depicted. When the condensation rate is constant (as is the case with the experimental set-up described above), the weight of the underlay sample increases linearly because more and more surface moisture accumulates on the underside of the sample.

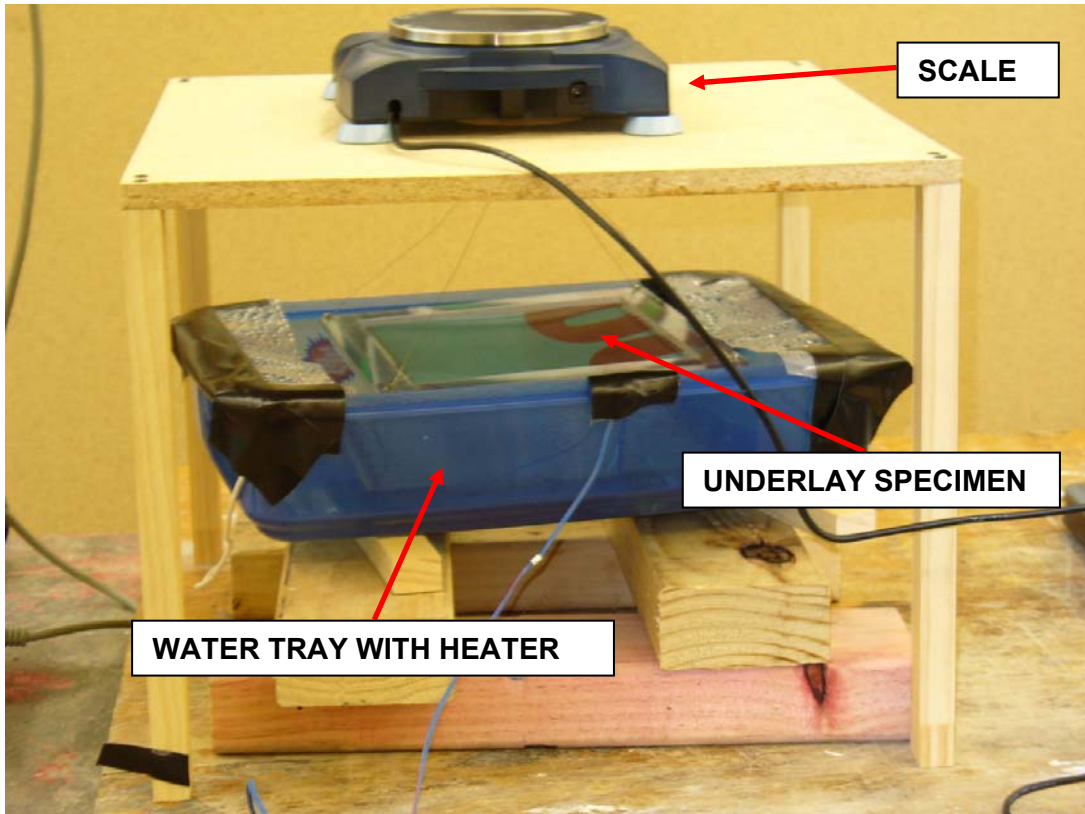


Figure 40: Experimental set-up for "Surface water no-drip test"



Figure 41: Detail of the Plexiglas frame supporting the underlay. The specimen is attached simply using double tape

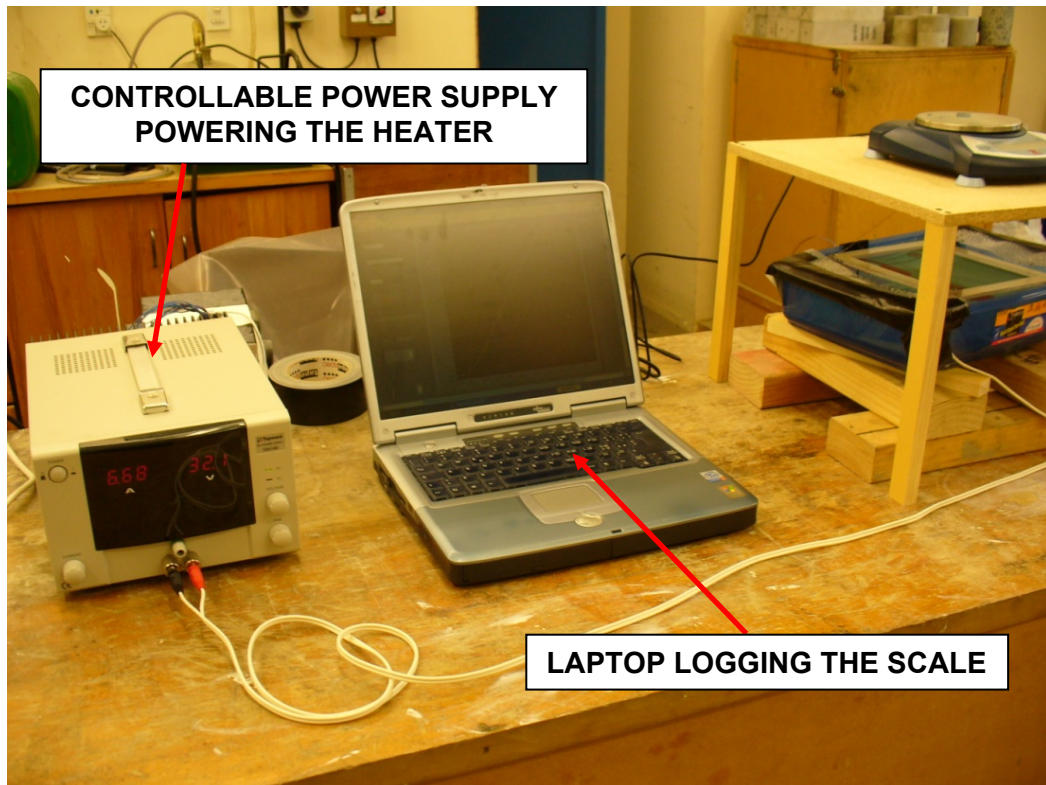


Figure 42: Part of the equipment controlling and logging the "Surface water no-drip test"

Drip does not start until the accumulation of condensation has not reached a certain threshold. When dripping starts, the amount of condensation on the underside of the sample starts growing at a slower rate than before because some water is lost through dripping.

The aim of the test is to quantify when drip starts, to give an indication of the maximum amount of condensation that can be held by surface tension before drip commences. In the test the sample is kept horizontal for simplicity. In the case of a real roof, in many cases, the underlay is on a slope. It is likely that the amount that can be held on the underside of a sloped underlay before any running (which often provokes dripping by the coalescing of droplets) occurs is less than the amount quantified by this test on horizontal underlays.

8.4 Results of the Surface water no-drip test

Applying the procedure proposed for the surface water no-drip test, the results shown in Figure 44 were obtained. As was expected, all underlays gain mass in a linear way until drip starts. The first part of all curves is quite similar. Since the experimental conditions are similar, the accumulation of condensation happens at similar rates. When drip starts, the slope of the curve changes. Moreover, entire water droplets are suddenly lost when drip starts and we can expect that the mass of the underlay changes quite suddenly. This is seen in Figure 44; the curves from smooth lines become more jagged and erratic.

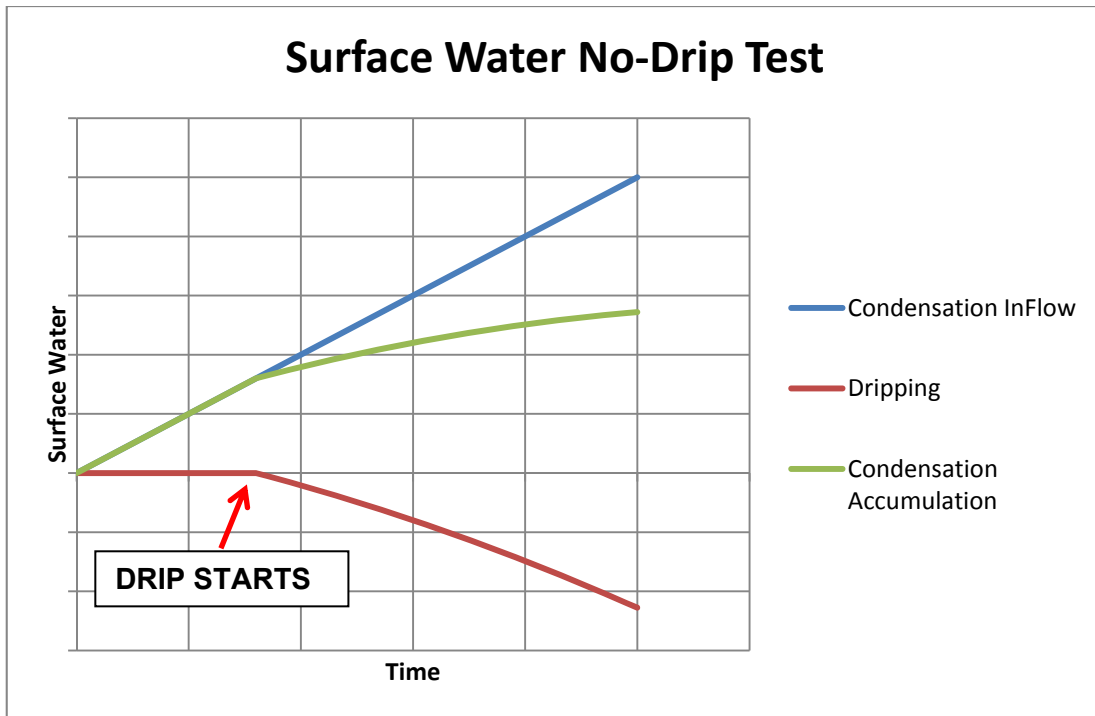


Figure 43: Theoretical interpretation of the surface water no drip test

If we assume that the first part of all curves (before drip starts) is linear, it is possible to extract the mass loss due to dripping (refer to Figure 43). The analysis of the results of the surface water no-drip test applied to several roof underlays is presented in Figure 45. The most important piece of information that can be extracted from Figure 45 is the time of drip start. What happens after drip starts is certainly interesting but not relevant for the test. The surface water no-drip test aims to probe how much moisture can be held by surface tension on the underside of the underlay without dripping and not how the amount of condensation evolves after drip occurs.

The time when drip starts is the time when the mass loss by drip (Figure 45) becomes different by zero. A visual inspection of the curve describing the mass loss by drip is sufficient to determine this time. Once this time has been determined, the corresponding condensation accumulation can be read from the raw data of the test (Figure 44). This value represents the accumulation of condensation at which drip commences and it is the main quantity measured by the surface water no-drip test.

8.5 Threshold for the Surface water no-drip test

The surface water no-drip test measures the maximum accumulation of condensation that can form on the underside of the underlay before any drip occurs. In order for the underlay to perform its function, this quantity should be larger than the maximum amount of condensation that is likely to accumulate on the underside of the underlay under frosty conditions. From a preliminary analysis of the data collected from the experimental test house under Wellington weather conditions, the maximum accumulation of condensation on the underside of the underlay has been found to be 15 g/m^2 . Allowing for more severe weather conditions found in other parts of New Zealand, this number informs a choice of 100 g/m^2 as the threshold to pass for the surface water no-drip test. This threshold could undergo modification when the results of more detailed analysis will be known. If a roof underlay can hold at least 100 g/m^2 of condensation on its underside by surface tension, the test has succeeded.

Table 12: Results of the surface water no-drip test for several roof underlays. The condensation accumulation is the maximum amount of condensation that can be held by surface tension by a roof underlay in a horizontal position before drip starts

Wrap	Drip Time (min)	Condensation Accumulation when drip starts(g)
Wrap C	65	170
Wrap D	85	280
Wrap E	65	180
Wrap F	85	320
Wrap J	55	320

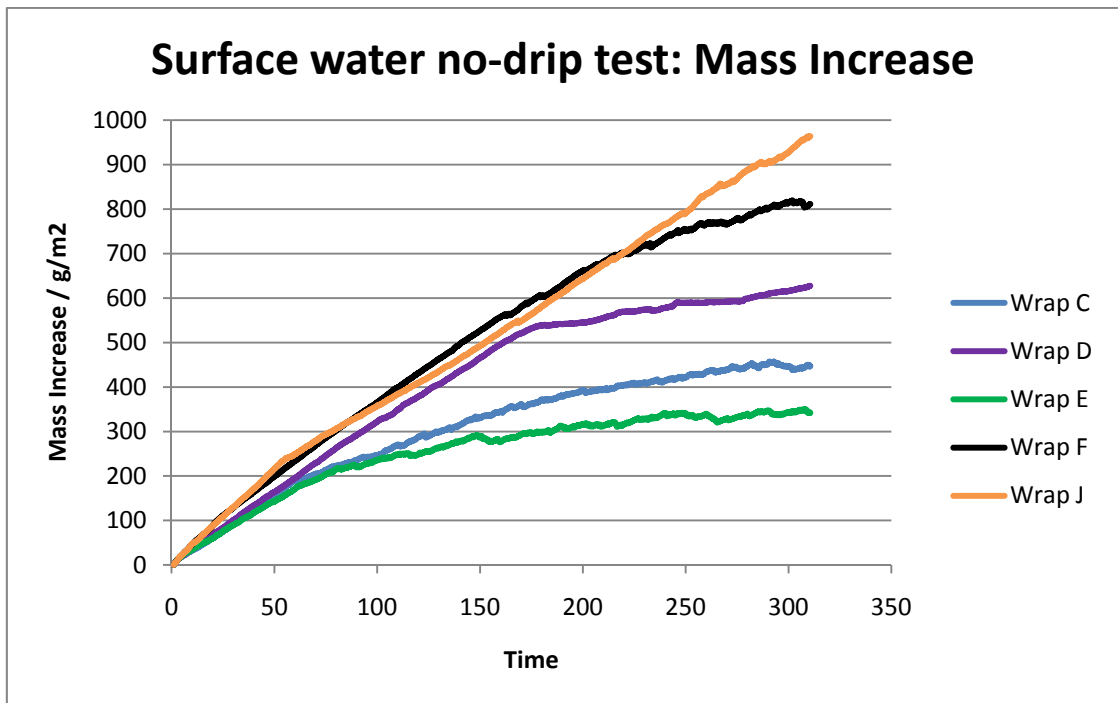


Figure 44 Surface water no-drip test: mass increase of different underlay samples

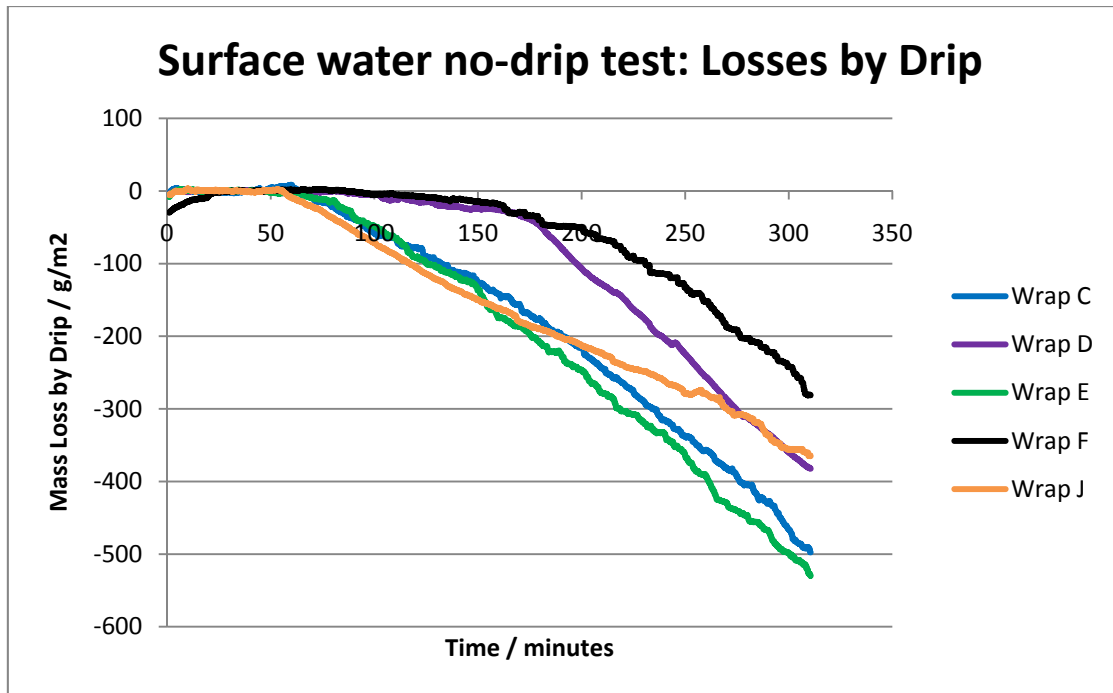


Figure 45 Surface water no-drip test: mass loss due to drip.

8.6 Conclusions

A new test for roof underlays is proposed as an alternative to the absorbency test described in AS/NZS 4201.6. This test probes the ability of a roof underlay to hold surface moisture on its underside. The test measures the maximum amount of condensation that can be held on the underside of the underlay before drip starts. In order to pass the drip test, this amount should be greater than 100 g/m².

9. SUMMARY OF FINDINGS

We find that all underlay tests in Standards AS/NZS 4200 and NZ S2295 serve a useful purpose except the absorption test. Since this test is found nowhere else in the world one wonders what its purpose is.

9.1 Condensation

The received wisdom is that the absorption test is supposed to ensure that roofing underlays are able to absorb condensation dripping from the underside of metal roofs, preventing it dripping deeper into the roof structure.

We find:

1. that there is no drip
2. that condensation under the roof moves to the lowest point of a metal roof
3. that if the underlay is in contact with the lowest point of the roof metal profile some of the condensation that has moved to there is transferred to the underlay
4. that any moisture that thus appears on the top of the underlay never penetrates through the underlay to the underside
5. that the underlay acts to shield the roof from moist air from below reducing or even preventing condensation from appearing under the roof
6. that much of the condensation thus appears under the underlay rather than under the roof.

The consequences of these findings are:

1. from finding 4 that, from the top, all underlays must prevent transfer of liquid through the underlay from top to bottom
2. from finding 6 that, from the bottom, the condensation appearing under the underlay must not drip deeper into the roof structure.

The tests needed to address these consequences are:

1. a head of water test specifying that no liquid must penetrate through the underlay under a head of one drop diameter, a few millimetres
2. from the bottom, a condensation test confirming that condensation forming under the underlay does not drip deeper into the roof structure.

Test details:

1. from the top the existing test for a 100mm head of water easily exceeds the requirements for a head of a few millimetres
2. from the bottom a new test is described that simulates condensation appearing on the bottom of the underlay and requires that the underlay can hold at least 100 g/m² by surface tension.

9.2 Solar driven moisture transfer

We find that solar driven moisture transfer is not an issue.

APPENDIX A SURFACE WATER NO-DRIP TEST

SURFACE WATER NO-DRIP TEST

1 SCOPE This test determines the maximum amount of water that can be held on the underside of a pliable building membrane before drip occurs.

2 APPARATUS The following apparatus is required.

- (a) **Container** – open top with approximate dimensions 250 x 250 x 50 mm. The container shall be impermeable and have an inner face non-reactive to water.
- (b) **Container guard area** – a 250 x 250 mm lid (of a material with similar properties as the walls of the container) with a concentric 220 x 220 mm hole.
- (c) **Distilled water**
- (d) **Controllable water heating system** – any water heating system able to heat and maintain the distilled water within the container at a temperature of 60 ± 1 °C (i.e. a resistive heater made of thin metallic wires whose voltage supply is controllable).
- (e) **Scale with underside hook and data logging capability** – accurate to 0.01 g.
- (f) **Thin square Plexiglas holding frame** – 200 x 200 mm square of Plexiglas (approximately 5 mm thick) with a concentric 150 x 150 mm square hole and with 4 very thin wires of equal length each connected at one end to a different corner of the holding frame and at the other end to a common point so to allow the holding frame to be hung to the underside hook of the scale.
- (g) **Scale frame to suspend the scale over the Container** – the scale frame should allow free access to the underside hook of the scale and hanging the Plexiglas holding frame to it. Enough vertical clearance is required in order to be able to suspend the Plexiglas holding frame over the container such that the guard area of the container and the Plexiglas holding frame are at the same height (within ± 2 mm).
- (h) **Steel ruler** – accurate to 1.0 mm.
- (i) **Double sided tape**

3 TEST SPECIMEN The test specimen shall be at least 1000 mm in length in machine direction, and be of full roll width.

4 PROCEDURE The method of test for surface water drip shall be conducted as described in this section. Steps (c), (d), (e) and (f) shall be conducted in a room at 23 ± 2 °C.

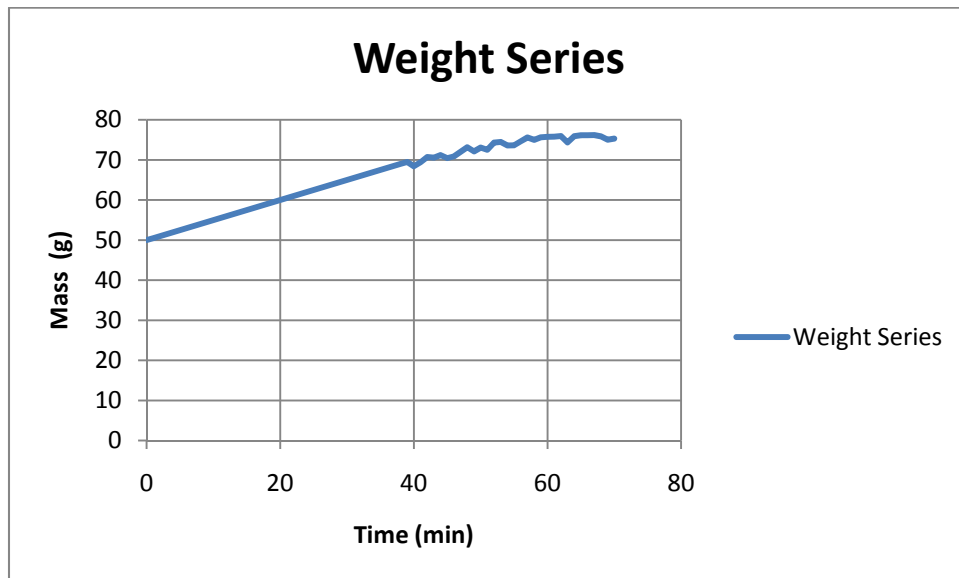
- (a) Cut 5 pieces, each 200 x 200 mm square with edges parallel and perpendicular to machine direction. To ensure squareness, the diagonals measurements should be equal to within 2 mm and the sides should be equal to within 1 mm. Alternately a template to the same limit may be used. The 5 test pieces shall be cut from the test specimen in a diagonal pattern, such that –
 - (1) The full width of the test specimen is uniformly sampled by centring the test pieces at equal distances; and

- (2) The test pieces are centred at least 200 mm apart in the machine direction.
- (b) For each specimen, attach four 200 mm strips of double sided tape on the underside of the Plexiglas holding frame along its outer edges and then use them to secure the specimen. Make sure that the specimen is aligned square on to the sides of the Plexiglas holding frame and that the upper and underside of the specimen are oriented as the pliable building membrane would be while in use.
 - (c) Fill the container with distilled water up to 20 mm from the top edge, put the guard area on and put the whole set-up under the scale frame supporting the scale such as to be vertically centred with the underside hook of the scale.
 - (d) Heat the water to its target temperature (60 ± 1 °C) and maintain that temperature for the whole duration of the experiment.
 - (e) Once the water temperature is under stable control at 60 ± 1 °C, tare the scale and only then hang the Plexiglas holding frame with the specimen to the underside hook of the scale. If needed, rotate the container until the 220 x 220 mm hole in the lid is aligned square with the Plexiglas holding frame. Make sure that the Plexiglas holding frame can hang freely from the underside hook of the scale and that it is at rest.
 - (f) Log the weight of the Plexiglas holding frame with the specimen at regular intervals (at least every 10 s) for 4 hours. Timestamp (in relative time, i.e. from the start of logging) each measurement with an accuracy of ± 1 s. Call the series of logged data the “weight series”.
 - (g) Calculating the amount of condensation accumulation when dripping just starts. The analysis of the time series of weight measurements shall be executed as follows:
 - (1) Subtract the initial weight measurement to the whole weight series. Call this the “weight increment series”.
 - (2) Take the weight increment measurements between 10 minutes and 30 minutes after the start of the test and compute the least-square linear interpolation through the data.
 - (3) Subtract the linear trend, computed in step (g) (2) above, from the weight increment series. Call this the “drip series”.
 - (4) Plot the drip series and determine the time when the drip series values becomes permanently negative. Call this the “reference time”.
 - (5) From the weight increment series, determine the weight increment corresponding to the reference time. This is considered as the amount of condensation accumulation on the underside of the 200 x 200mm specimen when dripping just starts. Call this the “test result”.
 - (h) Calculate the average of the 5 test results and divide the average by 0.04 to express in g/m^2 the amount of condensation accumulation when dripping just starts for the pliable building membrane.

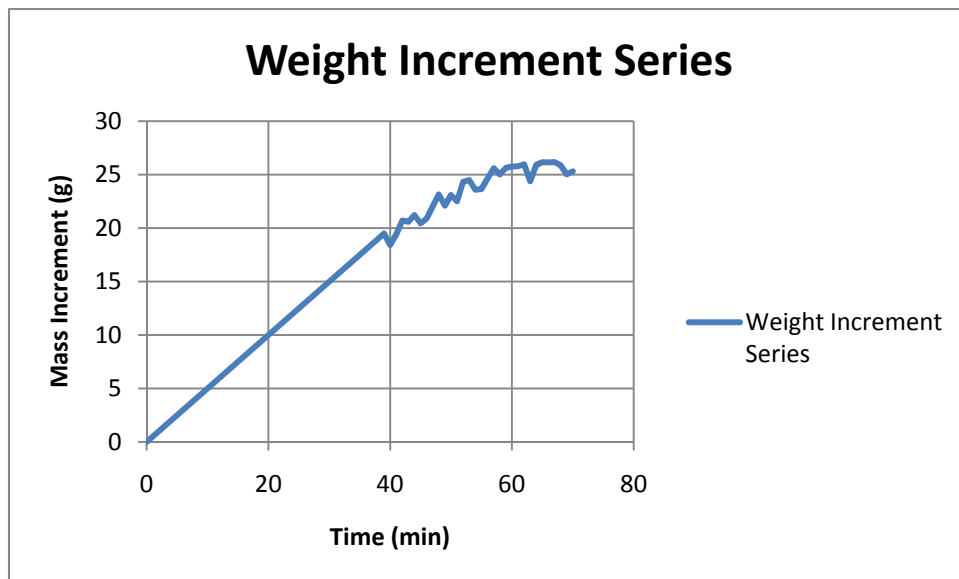
5 REPORTING The amount of condensation accumulation when dripping just starts for the pliable building membrane, rounded to the nearest 5 g/m^2 , shall be reported.

6 EXAMPLE

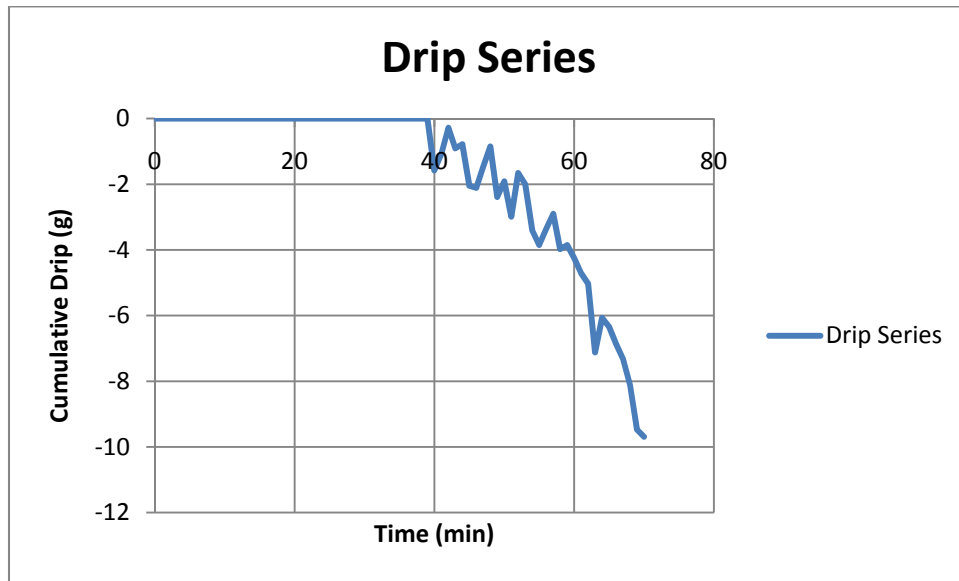
Step (f) Example of “Weight Series”



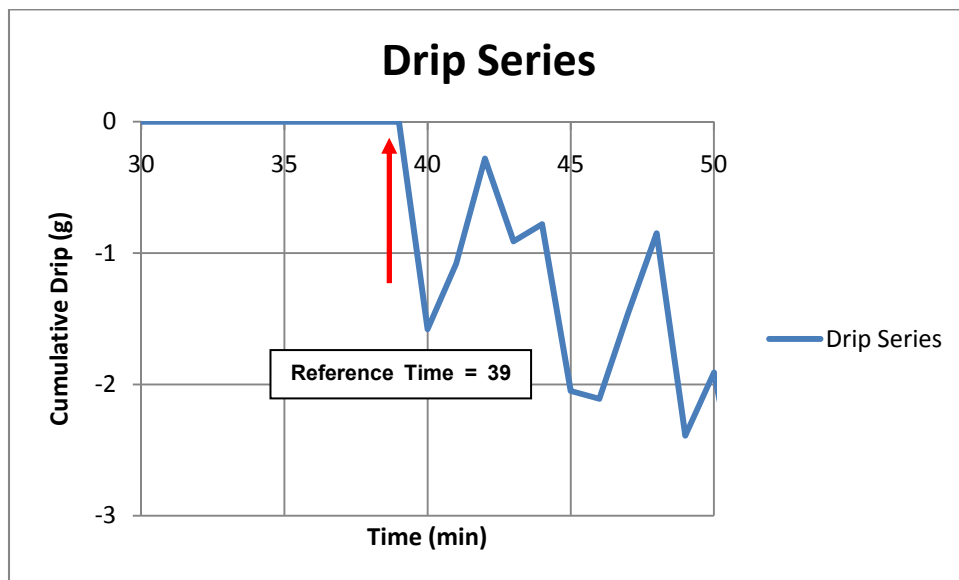
Step (g) (1) Corresponding “Weight Increment Series”



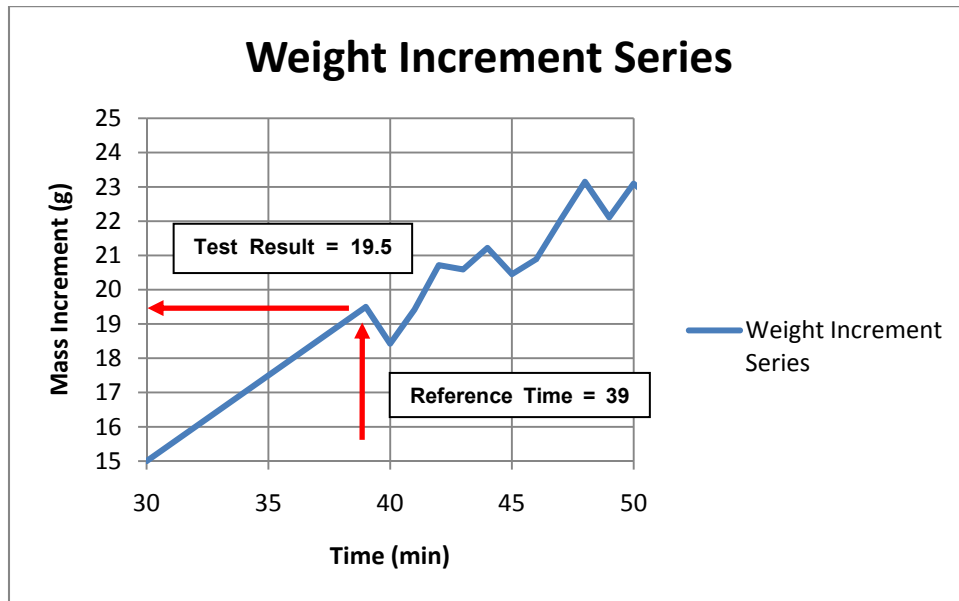
Step (g) (3) Corresponding “Drip Series”



Step (g) (4) Determining the “Reference Time”



Step (g) (5) Determining the “Test Result”



7 PICTURE OF A SET-UP FOR THE SURFACE WATER NO-DRIP TEST

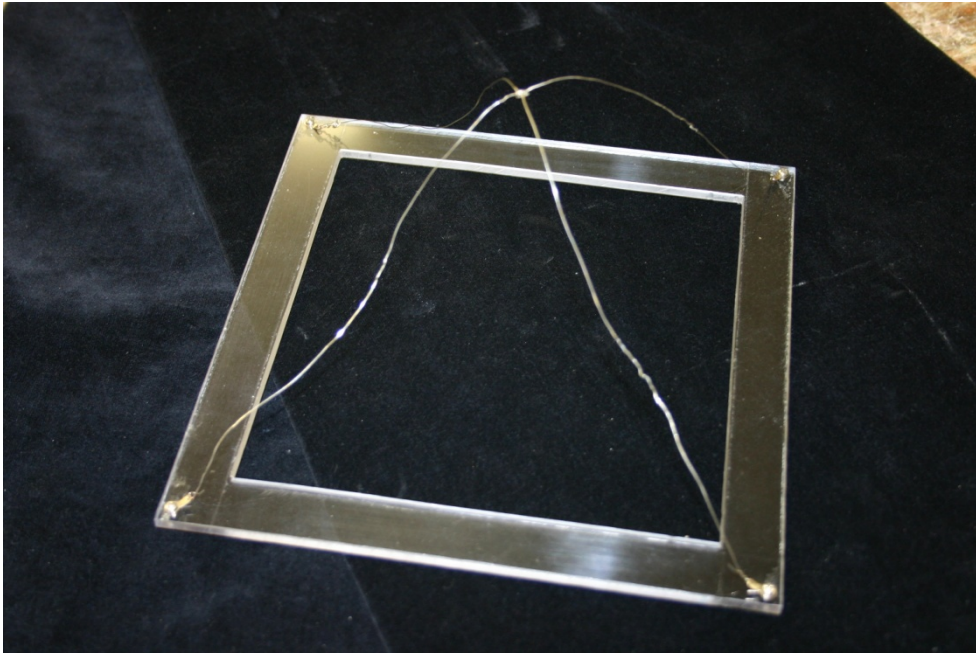


Figure 46: Thin square Plexiglas holding frame (no specimen attached)

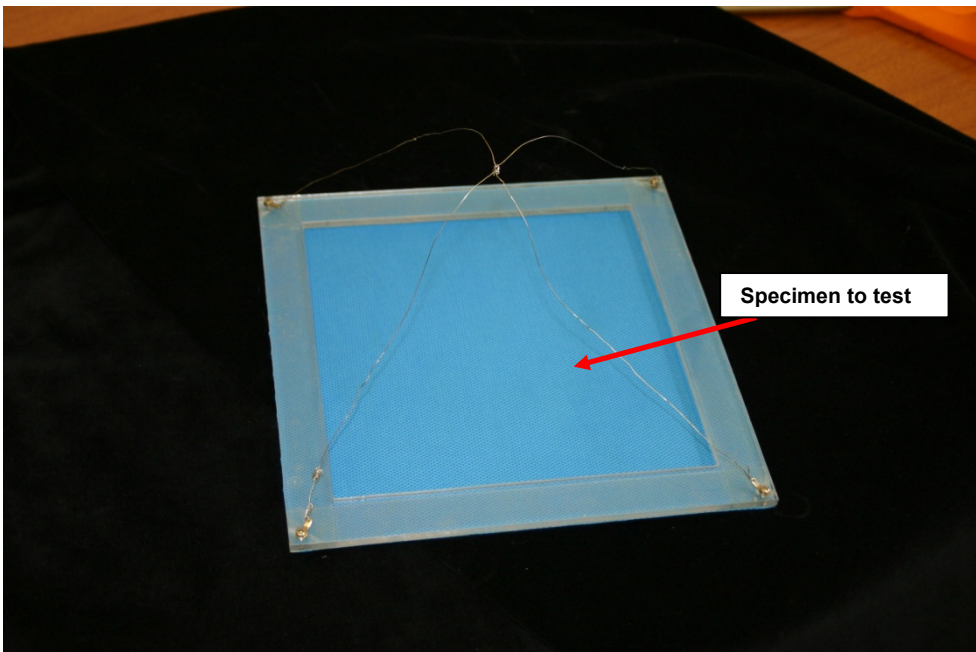


Figure 47: Thin square Plexiglas holding frame with specimen to test attached

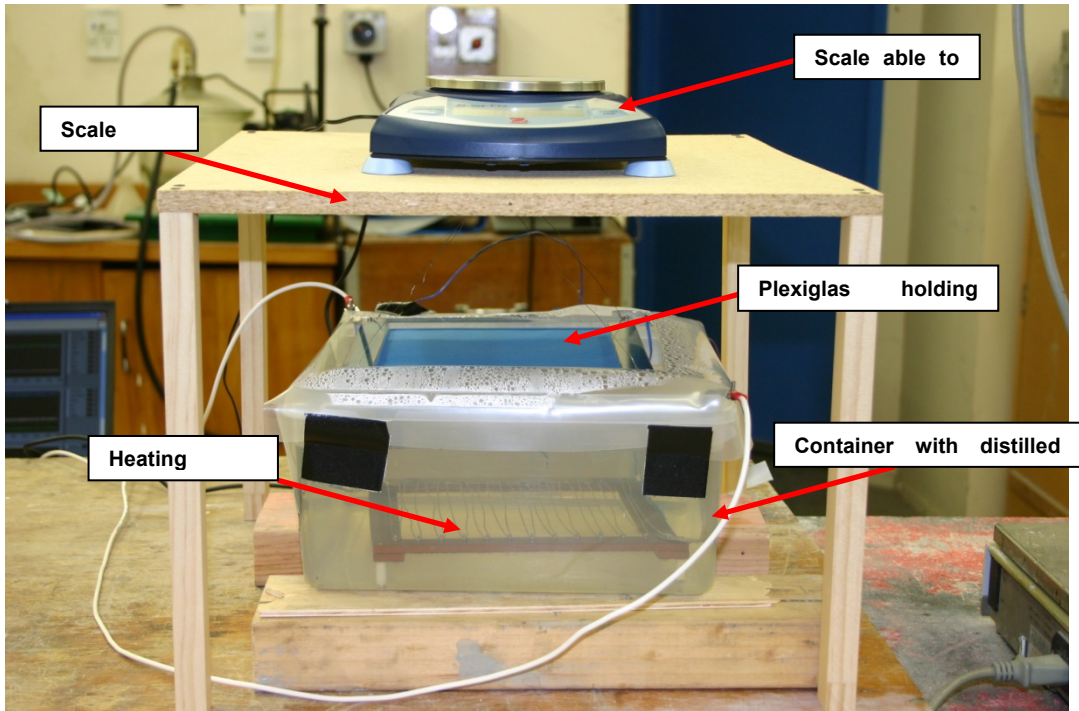


Figure 48: Experimental set-up. From top to bottom: scale sitting on scale frame, Plexiglas holding frame with specimen to test, container with distilled water and resistive heater.

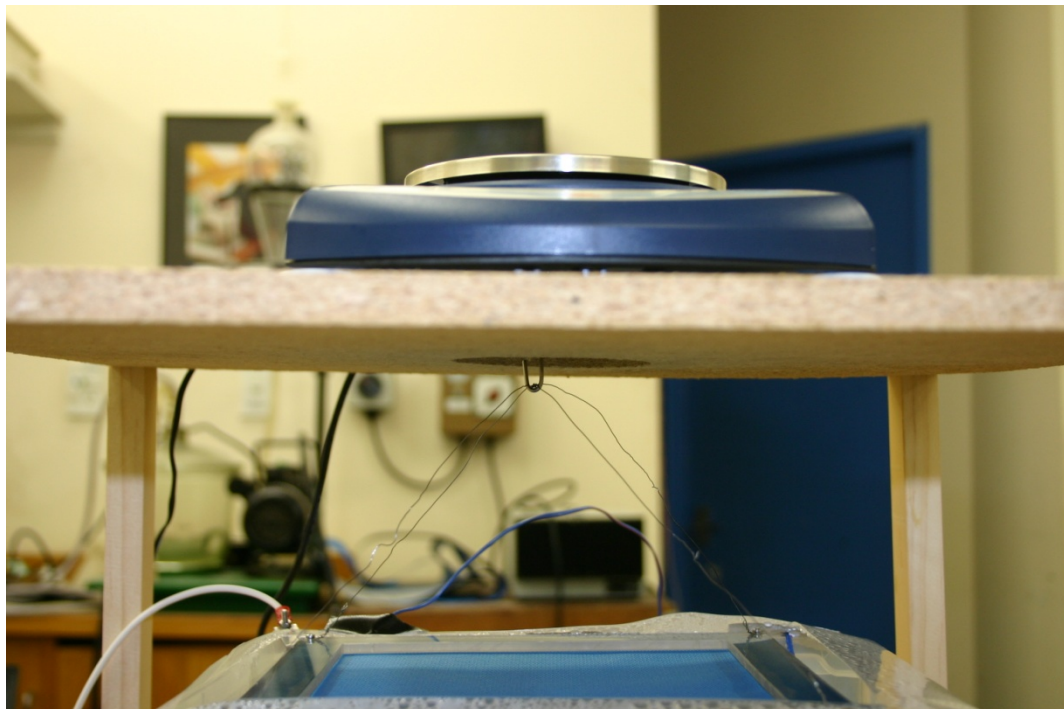


Figure 49: Detail of the underside hook of the scale supporting the Plexiglas holding frame with specimen to test.